Utilization of Mode-Match Technique for Calculating the Dispersion Characteristic of 2D Periodic Structure

by

Sitsofe Kudjoe Dorvlo

A Thesis

in

The Department

of

Electrical and Computer Engineering

Presented in Partial Fulfillment of the Requirements
for the Degree of Master of Applied Science (Electrical Engineering) at
Concordia University
Montreal, Quebec, Canada

April 2008

Your file Votre référence
ISBN: 978-0-494-40880-3
Our file Notre référence
ISBN: 978-0-494-40880-3

ABSTRACT

Utilization of Mode-Match Technique for Calculating the Dispersion Characteristic of 2D Periodic Structure

Sitsofe Kudjoe Dorvlo

In this work the Mode-Matching-Point-Matching (MM-PM) has been applied to determine the dispersion characteristics for a two-dimensional (2-D) structure. The 2-D structure is defined as a structure with a homogeneous dielectric substrate backed by a ground-plane on one side and an array of strip lines on the other. In this case, a strip line is assumed to have an infinitesimal small thickness.

The developed MM-PM technique uses two well documented methods: the mode-matching and point matching technique to solve for both the transverse electric (TE) and the transverse magnetic (TM) modes at an interface. The two methods together produce a set of equations which are expressed in a homogenous matrix form. Using singular value decomposition, the homogenous matrix is solved to produce the dispersive characteristics of the microstrip.

The generated numerical results for both the one-dimensional (1-D) and 2-D structures are compared to Ansoft Designer and Ansoft HFSS simulated results. Also experimental results from fabricated structures are compared to theoretical results. A good match is obtained from all the different results.

Overall the results are in general very good agreement. These results demonstrate that the MM-PM technique, characterized by its simplicity, can be used as a possible alternative method for the determination of dispersion characteristics of structures.

ACKNOWLEDGMENT

I would like to acknowledge the support, guidance and advice from my supervisor, Professor Abdel Razik Sebak, during the course of this research and my time at Concordia University.

I would also like to acknowledge Alper Ozturk and Aidin Mehdipour for their help in producing experimental data.

To my family

for their encouragement, support and endless

patience.

TABLE OF CONTENTS

TABLE OF FIGURES

LIST OF SYMBOLS

$\alpha_{mn}^{(i)}$	Attenuation constant corresponding to the nth Floquet harmonic [or nth mode] in the region i in the y direction
β_m	Phase constant of the m^{th} Floquet harmonic wave in the direction of periodicity (i.e. z direction)
β_n	Phase constant of the n^{th} Floquet harmonic wave in the direction of periodicity (i.e. x direction)
β_z	Phase constant of the wave in the z direction
$\beta_{m(i)}^{(e)}$	Phase constant for the TM mode in the region i in the z direction
$\beta_{x(i)}^{(e)}$	Phase constant for the TM mode in the region i in the x direction
$\beta_{m(i)}^{(h)}$	Phase constant for the TE mode in the region i in the z direction
$\beta_{x(i)}^{(h)}$	Phase constant for the TE mode in the region i in the x direction
ε_0	Free Space Permittivity
ε_r	Relative Permittivity in the region 2
μ_0	Free Space Permeability
σ_L	Smallest Singular Value
$\psi_i^{(e)}$	Scalar wave function for the TM mode in the region i
$\psi_{mn(i)}^{(e)}$	m-nth Floquet harmonic associated to the scalar wave function for the TM mode in the region i
$\psi_i^{(h)}$	Scalar wave function for the TE mode in the region i

$\psi^{(h)}_{mn(i)}$	m-nth Floquet harmonic associated to the scalar wave function for the T E mode in the region I
ω	Angular frequency
$A^{(e)}_{mn(i)}, B^{(e)}_{mn(i)}$	Unknown coefficient involved in the solution for the nth scalar function of $\psi^{(e)}_{n(i)}$
$A^{(h)}_{mn(i)}, B^{(h)}_{mn(i)}$	Unknown coefficient involved in the solution for the nth scalar function of $\psi^{(h)}_{n(i)}$
$A_{z(i)}$	z-component of the vector potential A in the region i
$A_{zmn(i)}$	m-nth Floquet harmonic associated to the z-component of the vector potential A in the region i
$E_{x(i)}$	Total Electric field in the region i in the x direction
$E^{(e)}_{m(i)}$	Electric field for the TM mode in the region i in the z direction
$E^{(e)}_{x(i)}$	Electric field for the TM mode in the region i in the x direction
$E^{(h)}_{m(i)}$	Electric field for the TE mode in the region i in the z direction
$E^{(h)}_{x(i)}$	Electric field for the TE mode in the region i in the x direction
f	Frequency
$F_{z(i)}$	z-component of the vector potential F in the region i
$F_{zmn(i)}$	m-nth Floquet harmonic associated to the z-component of the vector potential F in the region i
$H_{x(i)}$	Total magnetic field in the region i in the x direction

$H_{x(i)}^{(e)}$	Magnetic field for the TM mode in the region i in the x direction
$H_{x(i)}^{(h)}$	Magnetic field for the TE mode in the region i in the x direction
k_n	Phase constant (n^{th} eigenvalue) in the x-direction corresponding to the nth mode
k_0	Free space wavenumber
k_r	Wavenumber in the region 2

ABBREVIATIONS

EM	Electromagnetic
FDTD	Finite Difference Time Domain
FEM	Finite Element Method
FSS	Frequency Selective Surfaces
HFSS	High-Frequency Structure Simulator
IEM	Integral Equation Method
MM	Mode Matching
MOL	Method of Lines
PBG	Photonic Band Gap
PM	Point Matching
PMC	Perfect Magnetic Conductor
SIE	Singular Integral Equation Technique
SVD	Singular Value Decomposition
TE	Transverse Electric mode
TEM	Transverse Electric Magnetic mode
TM	Transverse Magnetic mode
UC-PBG	Uniplanar Compact Photonic Band-Gap

Chapter 1

INTRODUCTION

1.1 Motivation

Recently there has been a lot of interest focused on periodic structures called photonic bandgap (PBG), because of their ability to forbid propagation of electromagnetic waves for a given frequency range. This allows for passband or stopbands to be developed for guided waves through transmission lines. Thus there has been a lot of work done in incorporating the use of periodic structures in applications where propagation of electromagnetic waves is prevented at certain frequencies. Such applications include traveling wave slot, dipole arrays, log periodic antennas, phased arrays. These structures are usually referred to as EBG [1][2][3][4].

As the uses of periodic structures increase so does the need to develop methods of designing structures with pre-defined properties. One important property of periodic structures that allows for this is known as the dispersion characteristic. With this information we can determine the passband or stopband of a particular structure. Hence intensive work has been carried out into developing numerical method to determine the dispersion characteristic of periodic structures. Several of these methods are briefly introduced in this thesis. With each method there is an inherit problem which ranges from being mathematically complex to requiring a large amount of derivations to being computationally intensive.

This thesis looks at developing a mathematical model able to calculate the dispersion characteristics for a 2-dimensional (2-D) periodic structure. The 2-D structure under consideration is defined as a structure with a homogeneous dielectric substrate backed by a ground-plane on one side and an array of metal patches on the other. In this case, the metal patches are assumed to have an infinitesimal thickness. Accordingly, a simple mathematical formulation is used. A similar model will be introduced for a one dimensional (1-D) structure, involving simple mathematical formulation and very little computational time[6].

1.2 Aim of Thesis

The Mode-Matching-Point-Matching (MM-PM) technique uses the mode-matching technique, alongside the point matching technique to develop a mathematical model used to determine the dispersion characteristic of a 2-dimensional (2-D) periodic structure. The results are then compared with simulated results using commercially available software and also experimental data.

The MM-PM technique for 2-D structures is derived by first determining the electric and magnetic field equations as an expression of normal modes in each region. The electric and magnetic fields are then matched using appropriate boundary conditions to produce a set of equations. These equations are then transformed into an infinite set of homogenous equations of unknown variables via the conventional techniques of taking a scalar product with a complete set of functions for that particular problem. These functions take the form of $A(\beta, f) = 0$. The singular value decomposition method is used to solve these equations. The aim of this thesis is to validate the MM-PM technique through the

development of theoretical results using Matlab as the computational tool. Furthermore, the theoretical results for both the 1-D structure and the 2-D structure are compared with experimental results and to see if it is a good representation.

1.3 Brief Outline of Thesis

Chapter 2 contains the literature review. A brief but comprehensive review of photonic band-gap (PBG) structures focusing on unilateral compact PBG structures is undertaken. Following that, the mode-matching technique is introduced with an explanation as to how it is used. Similarly, Floquet's Theory is introduced and its implication to this work is explained. The effects of the boundary conditions on the system are also introduced. Also a possible application of this work is discussed.

The mathematical modeling behind developing the MM-PM method for the 2-D periodic structure can be found in Chapter 3. The structure under consideration consists of a dielectric substrate backed by a ground place and air with an infinite array of patches, perfect conductors at an interface.

The mathematical model, a set of equations for the MM-PM technique, is developed by applying mode matching with the required boundary conditions. The model is then coded using Matlab to generate numerical results, the dispersion characteristics.

These numerical results are detailed in Chapter 4. The validity of the MM-PM method is checked by varying different parameters and seeing the effects on the solution. The results are then compared with simulation produced with commercially available software. The final part of this chapter introduces an application for this work.

In the Chapter 5, we conclude with suggested improvements, and possible future work.

Chapter 2

LITERATURE REVIEW

2.1 Photonics Band-Gap Structures

Photonic band-gap (PBG) structures are periodic structures in which optical waves are forbidden in certain frequency bands. PBG structures can be of one-, two- or three-dimensional periodic structures. Due to the analogy between electromagnetic wave propagation in multidimensional periodic structures and electron wave propagation in crystals, PBG structures have found applications in both optics and microwave regimes.

Recently there has been interest in the area of photonic band-gap engineering where extensive research has been done in applying PBG phenomena for practical use in microwave antennas [2]. PBG structures are widely used for improving the electromagnetic performance in microwave circuits and antennas [2]. These structures, operating at microwave frequencies, usually consist of periodic arrays of metal patches patterned on a grounded dielectric substrate [2].

By properly designing a PBG structure, the performance of these devices can be controlled. PBG structures can be used to prevent the propagation of substrate waves in a frequency band. Another property of PBG is their behavior as an artificial perfect magnetic conductor, reflecting the incident plane wave without phase reversal. This permits the design of transverse electromagnetic TEM wave-guides and low-profile

antennas. PBG devices at microwave frequencies can be found in the following applications: - microstrip antennas, resonant cavities and filters [2].

The analysis of the electromagnetic band-gap structures produces two different pieces of information, the dispersion curve of the modes supported by the periodic device and the phase of the reflection coefficient of the structure under plane-wave excitation. The most useful information is the dispersion curve which indicates where the propagation of electromagnetic waves will operate.

PBG structures can be divided into three categories, one, two, and three dimensional categories as shown in Fig. 2-1. In the microwave community one and two-dimensional periodic structures have been under investigation for awhile. Recently, new concepts and ideas developed in the optics regime have sparked new interest in the microwave area. Among the new ideas, the most attractive to microwave engineers is the ability to forbid electromagnetic wave propagation in all or selected directions. A lot of research has been done in the application of these new concepts in the microwave and millimeter-wave domain [5]. Some of these concepts have resulted in the different applications of which PBG structures are being used. For example, one-dimensional periodic structures can be found in metallic waveguides which have slots cut in and are used as slotted-waveguide linear antennas. Other types of 1-D periodic structures include leaky-wave antennas based on either periodic surface corrugation or metal grating along a dielectric waveguide.

Two-dimensional (2-D) periodic structure, properties include a distinctive pass-band and stop-band, slow-wave effects, low attenuation in the pass-band, and suppression of

surface waves when serving as the ground plane of planar microstrip circuits [3]. Thus they have found applications in frequency - selective surfaces (FSS) and polarization diplexer designs [5]. They can also be found in applications such as slow-wave phase shifters, surface wave and leaky wave suppressors, high impedance ground planes as well as TEM waveguides [5].

Three-dimensional (3-D) periodic structures can be found in applications such as high-efficiency LEDs and nano-cavity lasers.

Recently, there has been great interest and extensive efforts in developing novel periodic structures for planar microwave circuits and antennas [5]. For example the ubiquitous high-low impedance microstrip low pass filter is a 1-D periodic structure. For these 1-D periodic structures, the term PBG can only be used in a relatively loose fashion.

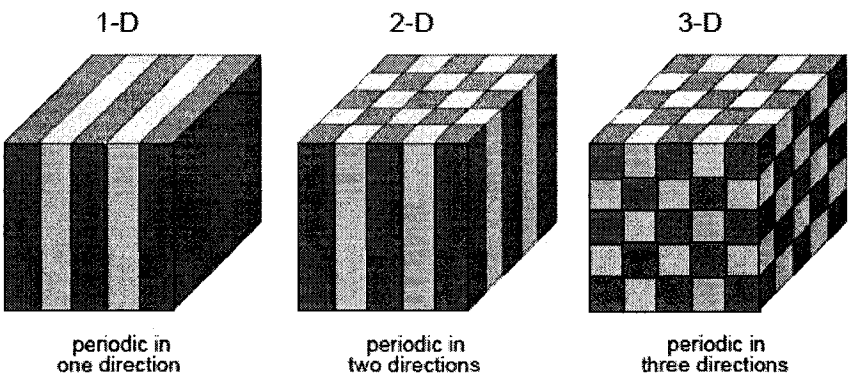

Fig. 2-1: Periodic Structure [5]

2.2 Uniplanar Compact Photonic Band-Gap Structure

In the quest to reduce the size of traditional periodic PBG structures, recent research efforts have developed compact structures periodically distributed in two dimensions.

These devices, referred to as Uniplanar Compact PBG (UC-PBG), can realize a 2-D periodic network without introducing vias, [4] and result in the reduction of the device size. The UC-PBG structures are structures which consist of a uniformly distributed periodic metallic pattern on one side of a dielectric slab. UC-PBGs thus exhibit properties of 2-D periodic structures. Moreover, the UC-PBG structure can also be used to realize a perfect magnetic conducting (PMC) surface, which finds applications in designing a TEM waveguide and a low profile cavity backed slot antenna [4].

In this thesis the primary focus is on a basic 2-D periodic structure which has one side of the dielectric backed by a ground plane and the other side an infinite array of patches (perfect conductors). Mohebbi [6] developed a system known as the mode-matching-point matching technique to calculate the dispersion characteristics of a microstrip line. It was then developed to accommodate a 1-dimensional periodic structure with periodicity in the x-plane. As part of the results section of this thesis we will compare results from MM-PM technique for 1-D structures with simulated results obtained from commercially available software and with measured results for identical structures.

2.3 Numerical Methods

In recent years, significant developments have been made in modeling techniques used to model opto-electronic components due to the introduction of commercially available computer-aided design software. These design tools have been significant in the study of optical components which vary from the optimization of designs, to the testing of new design concepts [7].

One modeling technique of significant interest is the mode solving technique which provides information to determine the mode(s) that can propagate in a given, uniform cross section of a wave guide structure [7]. Mode solving techniques are important parts of a design process since they provide information on the mode that propagates, the propagation constants and mode shapes, and, via overlap integrals, the relative modal excitations in a multimode guide in response to a given input field. For example, mode solving techniques can analyze a dielectric waveguide used in photonic integrated circuits which are known to propagate in a single mode but in some cases multimode or slightly multimode guides are involved in part of the device operation [7].

In applying mode solving techniques, we assume that the wave guide section is unaltered in the propagation direction [7]. Thus the direction of propagation can be determined based on the assumption that the variation in direction is exponential ($e^{i\beta z}$) where β, the propagation constant, is known. In summary, the mode solving techniques, for a waveguide cross-section and a specified value of operating frequency or wavelength, determine the values of β and the corresponding modal pattern for each desired mode.

The mode solving technique has further given birth to several numerical techniques to determine the dispersion characteristics of defined structures in both shielded and open environments. Since a lot of work has gone into the development of these formulations there exists a large number of publications on the different methods [8][9]. Listed below are a few of such methods.

- TEM approximations [8]
- Singular integral equation[10]

- Integral equation method[11]
- Method of lines[9]
- Spectral domain method[12]
- Finite difference method[9]
- Mode-matching[9]
- Finite difference time domain[13][14]
- Finite element method [15][16]

The finite difference time domain (FDTD) method is a grid based differential time domain numerical modeling method used in calculating the transverse electric and magnetic properties of structures. The FDTD works by discretizing the time-dependent Maxwell equations using the central difference approximation for the space and time partial derivatives [17]. These equations are then solved for the TE and TM cases alternatively [18] resulting in the dispersion characteristics. The FDTD is a very popular method used to calculate the dispersion characteristics of structures because it is a very versatile modeling technique to solve Maxwell's equations. Another advantage is that the FDTD is applied in the time domain it allows for propagation to be calculated over a large range of frequencies in a single simulation.

The finite element method (FEM) offers the possibility of a general tool for electromagnetic analysis, capable of handling arbitrary shapes and realistic materials. Finite elements works well in the analysis of problems with finite boundaries and the electric and magnetic fields extend over all space [19]. The FEM works by finding the approximate solution for partial differential equations, where it approximates these equations as ordinary differential equations. An example of the FEM can be found in

[20]. This example shows the analysis of the eigen-mode problem for uniform transmission lines to obtain the propagation constant for periodic structures [20].

The Method of Lines (MOL) is a technique again for solving partial differential equations where all but one dimension is discretized. This method uses a semi analytical approach, which yields accurate results, with less computational effects than other techniques [21]. The MOL permits the analysis of the hybrid modes that are supported by the waveguides under test. An advantage of the MOL is that it is a very comprehensive technique used to analyzing structures. I.e. it has the ability to analyze lossy waveguides and waveguides including metallization of finite thicknesses [22]. Also using the MOL method there is the added benefit that nonphysical or spurious modes do not appear in the analysis and that the method has no problem with relative convergences [21].

The integral equation method (IEM) is another popular method. IEM is been used in varies ways to formulate solutions for the scattering effect. One advantage of IEM is that it is able to be solved numerically within either the frequency or time domain [23]. An example of the use of this method is used in electromagnetics is in the solving of scattering from cavities in the conducting group plane. .

The singular integral equation technique (SIE) is used to solve many waveguide problems and has the advantage of characterizing the structure by a small order matrix, which can be used to produce accurate results for high-order modes. Another advantage is that the matrix elements are produces from analytical expressions, avoiding the need to calculate the infinite sums or numerical integrations that are involved in some methods [10].

The Spectral Domain Method is simply the Galerkin's approach but used in the Fourier transform or the spectral domain [24][25]. One of the advantages of this approach is that it is numerically more efficient than conventional methods that work directly in the space domain. This is due primarily to the fact that the process of Fourier transformation of the coupled integral equations in the space domain yields a pair of algebraic equations in the transform domain that are easier to handle [24][25]. Therefore one avoids the need to numerically evaluate complicated integrals, which can be extremely time consuming. Another benefit to the spectral domain method is that, eigenvalues for the propagation constants can be obtained from the determinantal equation [24].

The FDTD and the FEM are both intrinsically very rigorous but need long computational time to determine results since the longitudinal and transverse current distribution over the structure must be defined using a larger number of basis function to produce reasonable results. For the Finite Difference (FD) Method a large solution matrix is required to determine the zeros of the determinant to calculate the dispersion characteristics and so requires large computational power. The spectral domain method, documented in papers, is also limited as it requires a lengthy derivation processes in the formulation phase which is difficult to extend to complicated structures. The TEM approximation was one of the first methods used to determine dispersion characteristics, but as further research has been done and many numerical techniques have been developed it has been difficult to find published results that are in reasonable agreement. The IEM in many cases can be very flexible and efficient but it has some numerical difficulties in producing solutions.

2.3.1 The Mode Matching Technique

The mode-matching technique is a powerful method for analyzing periodic structures and waveguides with varying cross-sections using a straight forward mathematical formulation. This technique is useful when the geometry of the structure can be identified as an interface of two or more regions, each belonging to a separable coordinate system, as shown in Fig. 2-2 where A and B denotes two different regions. [6][26].

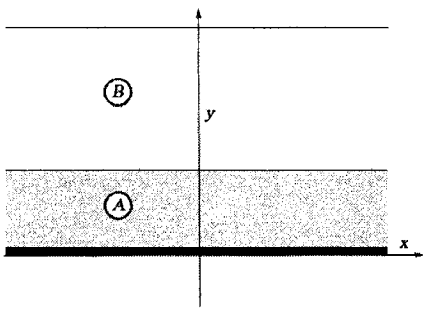

Fig. 2-2 Rectangular waveguide

In each region there exists a set of well-defined solutions of Maxwell's equations that satisfy all the boundary conditions except at the interface. The mode matching technique is based on the matching of the total mode fields at each junction between uniform sections. Thus by solving at the interface we can determine the electromagnetic characteristics of the device under investigation. The electromagnetic fields traveling along an axially periodic structure as guided waves are described by Floquet's theory.

The first step in the mode-matching procedure is the expansion of unknown fields in the individual regions, for example regions A and B in Fig. 2-2, in terms of their respective normal modes. Since the functional form of the normal modes is known, the problem is reduced to determining the set of modal coefficients associated with the field expansions

in various regions [26]. This procedure in conjunction with the orthogonality property of normal modes eventually leads to an infinite set of linear simultaneous equations for the unknown modal coefficients.

In a periodic structure, the field can be expanded to a complete set of vector wave functions. These functions are usually called modes. The amplitudes of the separate modes at the output of a junction can be deduced in terms of the amplitudes of the mode spectrum at the input to the junction. The strength of the mode-matching technique stems from the fact that the amplitudes of the modes can be expressed as the components of a scattering matrix. Each boundary along the patch has its own scattering matrix.

Extracting an exact solution is usually not possible since this is an infinite system of equations. Because of this, one has to use approximation techniques such as truncation or iteration. In adopting one of these methods, care need to be taken to ensure the accuracy of the approximated results because of the relative convergence problem found in the evaluation of the mode-matching equations.

2.4 Radiation Condition and Edge Condition

In certain problems the region of interest contains boundaries at infinity or contains geometrical singularities thus resulting in non unique mathematical solutions to Maxwell's equations. Therefore, to produce a unique solution that gives the anticipated results one has to add extra conditions. These conditions are in the form of radiation and edge conditions.

2.4.1 Radiation Condition

The radiation condition is the addition of a parameter that governs the effects of the field at infinity for sources in an unbounded space containing a finite region. These can be introduced in one of two forms [6][27].

In the case where the medium is lossy the fields are required to vanish. The second method is when the medium is lossless and isotropic. In this case the field at infinity is determined by the sommerfield radiation condition. This condition states that "The field at a large distance r from the source has a phase processing outward and has an amplitude that decreases at least as rapidly as r^{-1}" [27]. More precisely, any transverse components ℓ of the field (with respect to the r direction) must satisfy the conditions [27].

$$\lim_{r\to\infty}\left(\frac{\partial\psi}{\partial r}-ik\psi\right)=0 \tag{2.1}$$

where $k=\omega\sqrt{\mu\varepsilon}$ is the propagation constant of the medium.

In attempting to simplify the mathematics involved we chose to implement the medium lossless. Thus the propagation constant reduces to the phase constant as the attenuation constant is assumed to equal zero.

2.4.2 Edge Condition

The edge condition is defined by the following equation.

$$\int\left(\varepsilon|E|^2+\mu|H|^2\right)dv\to\theta_T\,[27] \tag{2.2}$$

θ_T denotes the total energy at the edge

This means that the electrical and magnetic energy stored near the edge must be finite. In the case of this work presented in this thesis, the edge condition does not have to be invoked to obtain a unique solution.

2.5 Floquet Theorem

Floquet's theory is a branch of the theory of ordinary differential equations relating to the class of solutions to linear differential equations. According to Floquet's theorem, each solution of an equation can be expressed as an exponential function and a periodic function [6][28]. In this thesis, the Floquet–Bloch expansion method uses an expression of the fields in terms of the Floquet space harmonics. Using this, the propagation of EM waves along periodic dielectric structures is formulated as a rigorous boundary value problem. When Floquet's Theorem is applied rigorously it produces very accurate results.

The Floquet Theorem is applied to periodic structures where it is infinitely periodic in both the x and z axes. For the sake of simplicity, we will keep the periodicity for both directions constant, d and consider square metal patches.

The following statements for periodic structures were derived from Floquet Theorem outlined in [29].

(I) The field (time-harmonic electromagnetic field) $E(x,y,z)$ and/or $H(x,y,z)$ along a periodic structure in two dimensions takes the form of

$$E(x,y,z) = e^{-\gamma(x+z)} E_p(x,y,z) \tag{2.3}$$

$$H(x,y,z) = e^{-\gamma(x+z)} H_p(x,y,z) \tag{2.4}$$

where E_p and H_p are periodic functions of x and z with periodicity d.

(II) The Floquet Theorem states that along the line of periodicity, at any point of the unit cell, the time electromagnetic field takes on exactly the same value as a similar point on other unit cells multiplied by the exponential $e^{-\gamma d}$, where $\gamma = \beta_n + \beta_m$. Therefore the field between $0 < z < L, 0 < x < L$ for $E(x,y,z)$ and $H(x,y,z)$ for a unit cell located at $L < z < 2L$, $L < x < 2L$ will have similar properties.

(III) The field in a periodic structure can now be represented as

$$E(x,y,z) = \sum_{m=-\infty}^{\infty} \sum_{n=-\infty}^{\infty} E_{pn}(x,y) e^{-j\beta_n z} e^{-j\beta_m x} \tag{2.5}$$

$$\text{where } \beta_n = \beta_z + \frac{2n\pi}{d},\ \beta_m = \beta_x + \frac{2m\pi}{d}.$$

The Floquet Theorem can be stated in the form of a Fourier series expansion. Reviewing [6] we see that the effect of reducing the truncation, that is, increasing the number of terms, improves the approximation to the function value. The only area of concern is at the extremities of the graph where Gibbs phenomenon becomes a factor. But as mentioned in [6] this would not be a problem since we would not be considering values at the extremes.

2.6 Ill Conditioned Matrix

An ill conditioned matrix is defined as a matrix where the condition number is very large. That is matrix A in $Ax = b$ is very sensitive to changes in A or b. If a matrix is ill-conditioned it can be difficult to find the solution to the system $Ax = b$ particularly when iterations are used to find the solution [30].

For example the following equation represents two simultaneous equations in the form of $Ax = b$

$$\begin{pmatrix} 1 & 2 \\ 2 & 4.0001 \end{pmatrix} \begin{pmatrix} x_1 \\ x_2 \end{pmatrix} = \begin{pmatrix} 3 \\ 6.0001 \end{pmatrix}. \tag{2.6}$$

The solution to this set of equation is x1 = x2=1 but if 4.0001 is rounded to 4.0 unsolvable equations are obtained. Leaving 4.0001 as is and rounding 6.0001 to 6, the solution of the equation become x1 = 3 and x2=0. And if 4.0001 and 6.0001 were rounded off to 4 and 6 respectively redundant, equations would be produced. Thus it can be seen that slight changes in the equations could cause significant changes in the solution.

Another way of obtaining ill-conditioned matrices is when the [A] matrix values vary by several orders of magnitude, this would also result in widely discrepant results due to small perturbations in the values of matrix [A][30]

Ill-conditioned matrices can create issues for iterative solvers because one has to guess an initial value and iterate to a certain tolerance value. This can cause solving the set of equations a lengthy process and in some cases this may not be acceptable [30].

One well known method of solving ill-conditioned matrices is the Singular Value Decomposition (SVD) [31]. This will be discussed in the next section.

2.7 Singular Value Decomposition (SVD)

There are many applications of existing numerical techniques for the analysis of microwave and millimeter-wave structures. Some of these numerical techniques lead to a homogenous equation of the form of $(A)\cdot x = 0$, where A is a complex matrix of size m x n ($m \geq n$) and x is an n-element column vector. In order to determine the solution of this equation, it is common practice to vary a (complex or real) parameter γ until the $\det(A(\gamma)) = 0$ for $\gamma = \gamma_0$. This constant could either represent the propagation constant, the effective permittivity or the cut-off frequency. In this thesis we will be focusing on the propagation constant [32][33].

The accuracy with which the above equation is solved is directly related to the accuracy with which the zeros of $\det(A(\gamma))$ can be detected. For most numerical techniques available this is a difficult problem due to the fact that the matrix A is an ill-conditioned matrix i.e. the $\det(A(\gamma))$ changes rapidly due to small changes of γ_0[33] . Therefore, the homogenous equations have to be solved using a search algorithm that operates in small step widths to detect the zeros. On a computer, the algorithm also has to be able to cope

with inaccuracies introduced by the numerical limits of the computer. This can therefore affect the numerical solution of the equations significantly.

To improve the solution of the homogenous equations, a method known as the singular value decomposition (SVD) is used [31]. The singular value decomposition is an important factorization method of rectangular real or complex matrices, with several applications in signal processing and statistics. SVD is a powerful algorithm for dealing with matrices that are either singular or numerically very close to singularity. It is demonstrated that by detecting the minima of the minimum singular value instead of the zeros of the system determinant the accuracy of the computation is increased. Similarly, the search algorithm is simplified and the accuracy of the computation increases.

2.7.1 Statement of the theorem

The singular value decomposition is defined as follows: Suppose M is an m-by-n matrix whose entries come from the field K, which is either the field of real numbers or the field of complex numbers, then there exists a factorization of the form [33]

$$M = U\Sigma V^* \tag{2.7}$$

where U is an m-by-m unitary matrix over K, the matrix Σ is m-by-n with nonnegative numbers on the diagonal and zeros off the diagonal, and V^* denotes the conjugate transpose of V, an n-by-n unitary matrix over K. Such a factorization is called a *singular-value decomposition* of M. The matrix V thus contains a set of orthonormal "input" or "analyzing" basis vector directions for M. The matrix U contains a set of orthonormal "output" basis vector directions for M. The matrix Σ contains the singular values, which

can be thought of as scalar "gain controls" by which each corresponding input is multiplied to give a corresponding output [31].

2.8 Applications

The formulation developed provides a means to analyze 2-D periodic structures, an array of microstrip patches mounted on a grounded dielectric substrate. An example of such a situation is the leaky wave antenna.

2.8.1 Leaky-Wave Antenna

Leaky wave antennas radiate microwave and millimeter wave energy from a series of metal strips mounted on a dielectric waveguide. It is excited by a horizontal infinitesimal dipole inside the substrate, which launches the leaky waves [34][35][36]. These antennas have the advantage of being structurally very simple and have simple frequency scanning properties [34]. Leaky wave antennas are also of interest because their ability to produce highly directive beams.

One common configuration for leaky wave antennas is similar to the structure that was analyzed in the formulation detailed above [34]. This structure can be seen again in Fig. 2-3, where the spatial distance of the structure is *'a'*, and the width of the patch is *'L'* both in the x direction. For the equivalent y direction the spatial distance is *'b'* and the width is *'w'*.

The leaky wave antenna structure behaves like a leaky parallel-plate waveguide, allowing radiation at a scan angle. This angle is primarily dependent upon the phase constant (β) of

the waveguide mode which is strongly dependent upon the substrate thickness [35] [37]. Knowledge of the propagation constant provides information about the beam direction. Specifically, the normalized phase constant β/k_o is related to the main beam direction i.e. the scan angle θ, and the normalized attenuation constant α/k_o, provides information on the beam width in the azimuth [34][35]. Using the phase information extracted by the formulations developed in this work, the main beam direction of the leaky-wave antenna can be determined.

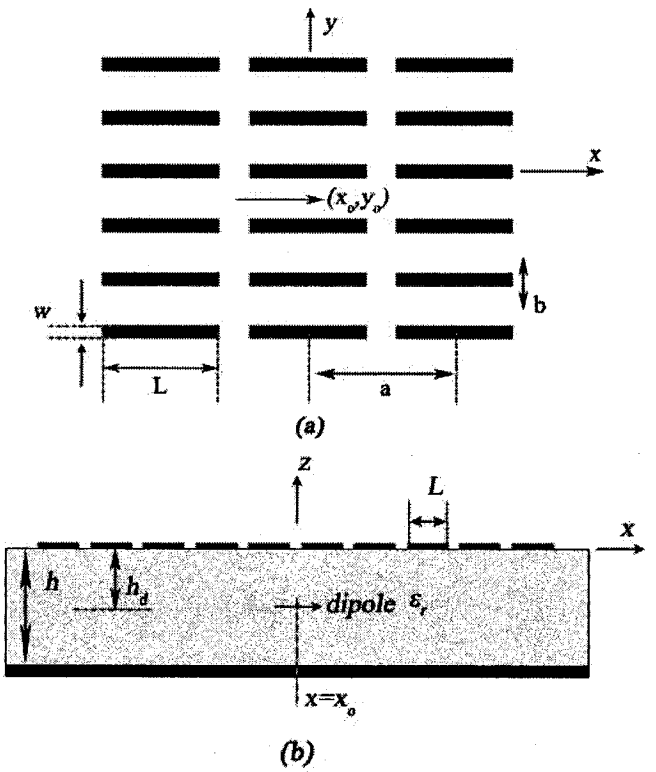

Fig. 2-3: Geometry of the 2-D periodic LWA. [34] (a) Top view. (b) Side view.

Chapter 3

FORMULATION FOR 2-D PERIODIC STRUCTURE

Due to the periodicity of the structure, the Floquet theorem can be applied and the electromagnetic problem reduces to the investigation of the unit cell of the periodic structure. The key to understanding periodic structures in two dimensions is to realize that the fields in 2D can be divided into two polarizations by symmetry [5]: TM^z (transverse magnetic), in which the magnetic field is in the (x-y) plane and the electric field is perpendicular (z); and TE^z (transverse electric), in which the electric field is in the (x-y) plane and the magnetic field is perpendicular. The use of Floquet's theorem reduces the analysis to a single cell of the propagating fields for both, - TE^z and TM^z polarizations.

3.1 Formulation

The cross section geometry of the device considered can be seen in

Fig. 3-1, where $2\times t$ is the width of the metal patch along x; $2\times L$ is the length of the unit cell along y; h is the height of the air substrate combined with that of the substrate; and d is the height of the dielectric substrate. Also regions 1 and 2 denote the dielectric and air substrate, respectively.

To simplify the analysis, and to obtain an accurate eigenvalue problem, a perfect electric conductor is placed parallel to, and at a large distance from the ground plane. The distance h is chosen large enough so that there is little or no effect on the guide properties from the conducting plane. In the structure, all components of the E and H fields will be found in the guided modes.

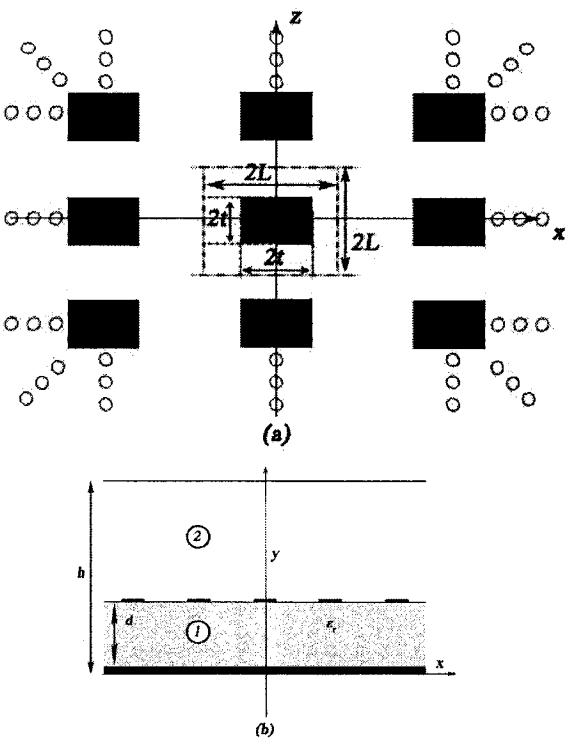

Fig. 3-1: Cross section of 2-D periodic structure (a) Top View (b) Side View

The incident wave on the device is a plane wave and the geometry of the scatterer is periodic in x with a period of L. The field is obtained at two arbitrary points, separated by a distance L along a line parallel to the x-axis. This means that the scattered field is calculated only in the basic period, $-L < x < L$ with the same is applied for the z direction.

To determine the dispersion characteristics of a periodic structure the following steps were followed. First the transverse electric (TE^z) and transverse magnetic (TM^z) fields were written using normal modes in each sub-region. Then the electric and magnetic fields were matched at the boundaries by applying the continuity conditions at the gap $|x| > t$ and the boundary condition on the strip $|x| < t$ at the interface $y = d$ [38]. Thirdly the produced equations were transformed into an infinite set of homogenous simultaneous equations that could be solved using singular value decomposition. It is important to note that care need be taken in choosing the appropriate truncation for the number of nodes for the relative convergence.

3.1.1 Assumption

In this analysis, it is assumed that the fields are time-harmonic, and the wave is traveling along the positive z direction with the objective to find the dispersion curve along this direction. Also, the regions are homogenous and source-free. The patches are perfect conductors with negligible thickness. The substrate is assumed to be a lossless dielectric. The geometry is expressed in rectangular coordinates, so we use rectangular coordinate system for this problem.

3.2 Electromagnetic Fields

TE^z modes are obtained if $\vec{A} = 0$ and $\vec{F} = \hat{a}_z F(x, y, z)$. Likewise for the TM^z modes, it can be obtained if $\vec{F} = 0$ and $\vec{A} = \hat{a}_z A(x, y, z)$ which in turn produces the following equations.

TE^z [39][40]	TM^z [39][40]	
$E_x = -\frac{1}{\varepsilon}\frac{\partial F_z}{\partial y}$	$E_x = -j\frac{1}{\omega\mu\varepsilon}\frac{\partial^2 A_z}{\partial x \partial z}$	(3.1a, b)
$E_y = \frac{1}{\varepsilon}\frac{\partial F_z}{\partial x}$	$E_y = -j\frac{1}{\omega\mu\varepsilon}\frac{\partial^2 A_z}{\partial y \partial z}$	(3.2a, b)
$E_z = 0$	$E_z = -j\frac{1}{\omega\mu\varepsilon}\left(\frac{\partial^2}{\partial z^2} + \beta^2\right)A_z$	(3.3a, b)
$H_x = -j\frac{1}{\omega\mu\varepsilon}\frac{\partial^2 F_z}{\partial x \partial z}$	$H_x = \frac{1}{\mu}\frac{\partial A_z}{\partial y}$	(3.4a, b)
$H_y = -j\frac{1}{\omega\mu\varepsilon}\frac{\partial^2 F_z}{\partial y \partial z}$	$H_y = -\frac{1}{\mu}\frac{\partial A_z}{\partial x}$	(3.5a, b)
$H_z = -j\frac{1}{\omega\mu\varepsilon}\left(\frac{\partial^2}{\partial z^2} + \beta^2\right)F_z$	$H_z = 0$	(3.6a, b)

To solve the above equations, the Helmholtz Equation $\nabla^2\vec{\psi} + \beta^2\vec{\psi} = 0$ was used, where ψ_z is a scalar function which could be either standing waves (sinusoidal) or traveling waves (exponential with complex arguments). Therefore

$$\psi_z(x,y,z) = f(x)g(y)h(z) \tag{3.7}$$

develops into

$$\psi_z(x,y,z) = \left[C_1\cos(\beta_y y) + D_1\sin(\beta_y y)\right]\left[C_2 e^{-j\beta_x x} + D_2 e^{+j\beta_x x}\right]\left[C_3 e^{-j\beta_z z} + D_3 e^{+j\beta_z z}\right] \tag{3.8}$$

Given that the source is located in a position where only the positively traveling wave was present, Equation 3.8 simplified to

$$\psi_z(x,y,z) = \left[C_1\cos(\beta_y y) + D_1\sin(\beta_y y)\right]\left[C_2 e^{-j\beta_x x}\right]\left[C_3 e^{-j\beta_z z}\right] \tag{3.9}$$

The auxiliary equation for the TE^z is as follows:

$$F_z(x,y,z)=\left[C_1\cos(\beta_y y)+D_1\sin(\beta_y y)\right]\left[C_2e^{-j\beta_x x}\right]\left[C_3e^{-j\beta_z z}\right] \tag{3.10}$$

In developing the transverse electric wave TE^z mode, the following conditions and assumption, that there was no electric field present at the boundaries of the region were used. Thus given the boundary conditions

$$\begin{aligned} E_x(x,y=0,z)&=E_x(x,y=h,z)=0\\ E_z(x,y=0,z)&=E_z(x,y=h,z)=0 \end{aligned} \tag{3.11}$$

The auxiliary equation for the TE^z is:

$$F_z(x,y,z)=\left[C_1\cos(\beta_y y)\right]\left[C_2e^{-j\beta_x x}\right]\left[C_3e^{-j\beta_z z}\right]. \tag{3.12}$$

For the respective regions the auxiliary equations for the TE^z is as follows

region 1: $$F_{z1}(x,y,z)=\left[C_1\cos(\beta_y y)\right]\left[C_2e^{-j\beta_x x}\right]\left[C_3e^{-j\beta_z z}\right] \tag{3.13}$$

region 2: $$F_{z2}(x,y,z)=\left[C_1\cos(\beta_y (h-y))\right]\left[C_2e^{-j\beta_x x}\right]\left[C_3e^{-j\beta_z z}\right]. \tag{3.14}$$

Likewise for calculating the transverse magnetic wave TM^z modes, its corresponding auxiliary equation is as follows:

$$A_z(x,y,z)=\left[C_1\cos(\beta_y y)+D_1\sin(\beta_y y)\right]\left[C_2e^{-j\beta_x x}\right]\left[C_3e^{-j\beta_z z}\right]. \tag{3.15}$$

Using the same boundary conditions as used for the TE^z mode the auxiliary equation simplifies to

$$A_z(x,y,z)=\left[D_1\sin(\beta_y y)\right]\left[C_2e^{-j\beta_x x}\right]\left[C_3e^{-j\beta_z z}\right] \tag{3.16}$$

For the respective region the equations are as follows

region 1: $$A_{z1}(x,y,z)=[D_1\sin(\beta_y y)][C_2e^{-j\beta_x x}][C_3e^{-j\beta_z z}] \quad (3.17)$$

region 2: $$A_{z2}(x,y,z)=[D_1\sin(\beta_y (h-y))][C_2e^{-j\beta_x x}][C_3e^{-j\beta_z z}] \quad (3.18)$$

The geometry for the two-dimensional scattering by an infinite periodic structure is shown in Fig. 3-2.

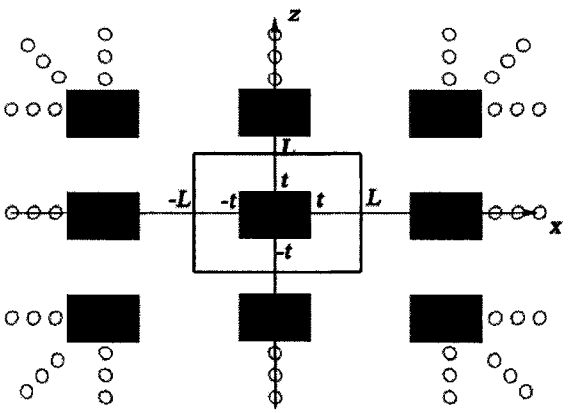

Fig. 3-2: Cross section of a periodic array of rectangular patch

The phase constants in x-direction and z-direction, according to the Floquet theorem, can be expressed by $\beta_n = \beta_x + \frac{2\pi n}{2L_x}$ and $\beta_m = \beta_z + \frac{2\pi m}{2L_z}$ respectively.

Therefore phase constant in the y- direction can then be expressed as

$$\alpha_{nm} = -j\beta_y = \sqrt{(\beta_n^{\,2} + \beta_m^{\,2}) - \beta^2} \quad (3.19)$$

To satisfy the boundary conditions at the interface between the dielectric and air, the total transverse scalar functions of $F_z(x,y,z)$ must be written as the summation of F_z. After some rearrangements, expanding in terms of the Floquet modes and using A_{nm} for region 1, Fig. 2-3(b) to symbolize constants equation 3.13 becomes:

$$F_{z1}(x,y,z)=\sum_{n=-\infty}^{\infty}\sum_{n=-\infty}^{\infty}A_{nm}\cosh(\alpha_{nm}y)e^{-j\beta_n x}e^{-j\beta_m z}\,. \tag{3.20}$$

Following a similar method for equation 3.14 the following is formed

$$A_{z1}(x,y,z)=\sum_{n=-\infty}^{\infty}\sum_{n=-\infty}^{\infty}A_{nm}\sinh(\alpha_{nm}y)e^{-j\beta_n x}e^{-j\beta_m z}\,. \tag{3.21}$$

Again this is repeated for region 2, with B_{nm} used to symbolize constants, equations 3.15 and 3.16 transform to the following respectively,

$$F_{z2}(x,y,z)=\sum_{n=-\infty}^{\infty}\sum_{n=-\infty}^{\infty}B_{nm}\cosh(\alpha_{nm}(h-y))e^{-j\beta_n x}e^{-j\beta_m z} \tag{3.22}$$

$$A_{z2}(x,y,z)=\sum_{n=-\infty}^{\infty}\sum_{n=-\infty}^{\infty}B_{nm}\sinh(\alpha_{nm}(h-y))e^{-j\beta_n x}e^{-j\beta_m z} \tag{3.23}$$

Substituting the auxiliary equations back into the Floquet harmonic equations the following were developed.

For the Transverse Electric Wave TE^z Modes in Region 1

$$E_x=-\frac{1}{\varepsilon_1}\sum_{m=-\infty}^{\infty}\sum_{n=-\infty}^{\infty}A_{nm}{}^{(h)}\alpha_{nm}\sinh(\alpha_{nm}{}^{(1)}y)e^{-j\beta_n x}e^{-j\beta_m z} \tag{3.24}$$

$$E_y=-j\frac{1}{\varepsilon_1}\sum_{m=-\infty}^{\infty}\sum_{n=-\infty}^{\infty}A_{nm}{}^{(h)}\beta_n\cosh(\alpha_{nm}{}^{(1)}y)e^{-j\beta_n x}e^{-j\beta_m z} \tag{3.25}$$

$$E_z=0 \tag{3.26}$$

$$H_x=j\frac{1}{\omega\mu\varepsilon_1}\sum_{m=-\infty}^{\infty}\sum_{n=-\infty}^{\infty}A_{nm}{}^{(h)}\beta_n\beta_m\cosh(\alpha_{nm}{}^{(1)}y)e^{-j\beta_n x}e^{-j\beta_m z} \tag{3.27}$$

$$H_y=-\frac{1}{\omega\mu\varepsilon_1}\sum_{m=-\infty}^{\infty}\sum_{n=-\infty}^{\infty}A_{nm}{}^{(h)}\beta_m\alpha_{nm}{}^{(1)}\sinh(\alpha_{nm}{}^{(1)}y)e^{-j\beta_n x}e^{-j\beta_m z} \tag{3.28}$$

$$H_z=-j\frac{1}{\omega\mu\varepsilon_1}\left(\sum_{n=-\infty}^{\infty}\sum_{n=-\infty}^{\infty}\left(\beta_{(1)}{}^2-\beta_m{}^2\right)A_{nm}{}^{(h)}\cosh\left(\alpha_{nm}{}^{(1)}y\right)e^{-j\beta_n x}e^{-j\beta_m z}\right) \tag{3.29}$$

In region 2 for the transverse electric mode,

$$E_x = \frac{1}{\varepsilon_2}\sum_{m=-\infty}^{\infty}\sum_{n=-\infty}^{\infty} B_{nm}{}^{(h)}\alpha_{nm}{}^{(2)}\sinh(\alpha_{nm}{}^{(2)}(h-y))e^{-j\beta_n x}e^{-j\beta_m z} \tag{3.30}$$

$$E_y = -j\frac{1}{\varepsilon_2}\sum_{m=-\infty}^{\infty}\sum_{n=-\infty}^{\infty} B_{nm}{}^{(h)}\beta_n\cosh(\alpha_{nm}{}^{(2)}(h-y))e^{-j\beta_n x}e^{-j\beta_m z} \tag{3.31}$$

$$E_z = 0 \tag{3.32}$$

$$H_x = j\frac{1}{\omega\mu\varepsilon_2}\sum_{m=-\infty}^{\infty}\sum_{n=-\infty}^{\infty} B_{nm}{}^{(h)}\beta_n\beta_m\cosh(\alpha_{nm}{}^{(2)}(h-y))e^{-j\beta_n x}e^{-j\beta_m z} \tag{3.33}$$

$$H_y = \frac{1}{\omega\mu\varepsilon_2}\sum_{m=-\infty}^{\infty}\sum_{n=-\infty}^{\infty} B_{nm}{}^{(h)}\beta_m\alpha_{nm}{}^{(2)}\sinh(\alpha_{nm}{}^{(2)}(h-y))e^{-j\beta_n x}e^{-j\beta_m z} \tag{3.34}$$

$$H_z = -j\frac{1}{\omega\mu\varepsilon_2}\left(\sum_{n=-\infty}^{\infty}\sum_{n=-\infty}^{\infty}\left(\beta_{(2)}{}^2-\beta_m{}^2\right)B_{nm}\cosh\left(\alpha_{nm}{}^{(2)}(h-y)\right)e^{-j\beta_n x}e^{-j\beta_m z}\right) \tag{3.35}$$

Transverse Magnetic Wave TM^z modes in region 1 are

$$E_x = j\frac{1}{\omega\mu\varepsilon_1}\sum_{m=-\infty}^{\infty}\sum_{n=-\infty}^{\infty} A_{nm}{}^{(e)}\beta_n\beta_m\sinh(\alpha_{nm}{}^{(1)}y)e^{-j\beta_n x}e^{-j\beta_m z} \tag{3.36}$$

$$E_y = -\frac{1}{\omega\mu\varepsilon_1}\sum_{m=-\infty}^{\infty}\sum_{n=-\infty}^{\infty} A_{nm}{}^{(e)}\beta_m\alpha_{nm}{}^{(1)}\cosh(\alpha_{nm}{}^{(1)}y)e^{-j\beta_n x}e^{-j\beta_m z} \tag{3.37}$$

$$E_z = -j\frac{1}{\omega\mu\varepsilon_1}\left(\sum_{m=-\infty}^{\infty}\sum_{n=-\infty}^{\infty}\left(\beta_{(1)}{}^2-\beta_m{}^2\right)A_{nm}{}^{(e)}\sinh\left(\alpha_{nm}{}^{(1)}y\right)e^{-j\beta_n x}e^{-j\beta_m z}\right) \tag{3.38}$$

$$H_x = \frac{1}{\mu}\sum_{m=-\infty}^{\infty}\sum_{n=-\infty}^{\infty} A_{nm}{}^{(e)}\alpha_{nm}{}^{(1)}\cosh(\alpha_{nm}{}^{(1)}y)e^{-j\beta_n x}e^{-j\beta_m z} \tag{3.39}$$

$$H_y = j\frac{1}{\mu}\sum_{m=-\infty}^{\infty}\sum_{n=-\infty}^{\infty} A_{nm}{}^{(e)}\beta_n\sinh(\alpha_{nm}{}^{(1)}y)e^{-j\beta_n x}e^{-j\beta_m z} \tag{3.40}$$

$$H_z = 0. \tag{3.41}$$

And in region 2

$$E_x = j\frac{1}{\omega\mu\varepsilon_2}\sum_{m=-\infty}^{\infty}\sum_{n=-\infty}^{\infty} B_{nm}{}^{(e)}\beta_n\beta_m\sinh(\alpha_{nm}{}^{(2)}(h-y))e^{-j\beta_n x}e^{-j\beta_m z} \tag{3.42}$$

$$E_y = \frac{1}{\omega\mu\varepsilon_2}\sum_{m=-\infty}^{\infty}\sum_{n=-\infty}^{\infty} B_{nm}{}^{(e)}\beta_m\alpha_{nm}{}^{(2)}\cosh(\alpha_{nm}{}^{(2)}(h-y))e^{-j\beta_n x}e^{-j\beta_m z} \tag{3.43}$$

$$E_z = -j\frac{1}{\omega\mu\varepsilon_2}\left(\sum_{m=-\infty}^{\infty}\sum_{n=-\infty}^{\infty}\left(\beta_{(2)}{}^2-\beta_m{}^2\right)B_{nm}{}^{(e)}\sinh\left(\alpha_{nm}{}^{(2)}(h-y)\right)e^{-j\beta_n x}e^{-j\beta_m z}\right) \tag{3.44}$$

$$H_x = -\frac{1}{\mu}\sum_{m=-\infty}^{\infty}\sum_{n=-\infty}^{\infty} B_{nm}{}^{(e)}\alpha_{nm}{}^{(2)}\cosh(\alpha_{nm}{}^{(2)}(h-y))e^{-j\beta_n x}e^{-j\beta_m z} \tag{3.45}$$

$$H_y = j\frac{1}{\mu}\sum_{m=-\infty}^{\infty}\sum_{n=-\infty}^{\infty} B_{nm}{}^{(e)}\beta_n \sinh(\alpha_{nm}{}^{(2)}(h-y))e^{-j\beta_n x}e^{-j\beta_m z} \tag{3.46}$$

$$H_z = 0. \tag{3.47}$$

For the sake of simplicity, we can consider the new variables $\frac{A_{nm}^{(h)}}{\varepsilon_r} \to A_{nm}^{(h)}$ and $\frac{A_{nm}^{(e)}}{\varepsilon_r} \to A_{nm}^{(e)}$ instead of the previous $A_{nm}^{(h)}$ and $A_{nm}^{(e)}$ likewise for $B_{nm}^{(h)}$ and $B_{nm}^{(e)}$, $\frac{B_{nm}^{(h)}}{\varepsilon_r} \to B_{nm}^{(h)}$ and $\frac{B_{nm}^{(e)}}{\varepsilon_r} \to B_{nm}^{(e)}$. The equations also have been normalized by a factor of $\left(\frac{-1}{\omega\mu_0\varepsilon_0}\right)$.

The final fields are the superposition of TE and TM fields:

$$E_{x1} = \sum_{m=-\infty}^{\infty}\sum_{n=-\infty}^{\infty}\left(\omega\mu_0 A_{nm}{}^{(h)}\alpha_{nm} - jA_{nm}{}^{(e)}\beta_n\beta_m\right)\sinh(\alpha_{nm}{}^{(1)}y)e^{-j\beta_n x}e^{-j\beta_m z} \tag{3.48}$$

$$E_{x2} = -\sum_{m=-\infty}^{\infty}\sum_{n=-\infty}^{\infty}\left(jB_{nm}{}^{(e)}\beta_n\beta_m + \omega\mu_0 B_{nm}{}^{(h)}\alpha_{nm}{}^{(2)}\right)\sinh(\alpha_{nm}{}^{(2)}(h-y))e^{-j\beta_n x}e^{-j\beta_m z} \tag{3.49}$$

$$E_{y1} = \sum_{m=-\infty}^{\infty}\sum_{n=-\infty}^{\infty}\left(A_{nm}{}^{(e)}\beta_m\alpha_{nm}{}^{(1)} - j\omega\mu_0 A_{nm}{}^{(h)}\beta_n\right)\cosh(\alpha_{nm}{}^{(1)}y)e^{-j\beta_n x}e^{-j\beta_m z} \tag{3.50}$$

$$E_{y2} = \sum_{m=-\infty}^{\infty}\sum_{n=-\infty}^{\infty}\left(j\omega\mu_0 B_{nm}{}^{(h)}\beta_n - B_{nm}{}^{(e)}\beta_m\alpha_{nm}{}^{(2)}\right)\cosh(\alpha_{nm}{}^{(2)}(h-y))e^{-j\beta_n x}e^{-j\beta_m z} \tag{3.51}$$

$$E_{z1} = j\left(\sum_{m=-\infty}^{\infty}\sum_{n=-\infty}^{\infty}\left(\beta_{(1)}{}^2 - \beta_m{}^2\right)A_{nm}{}^{(e)}\sinh\left(\alpha_{nm}{}^{(1)}y\right)e^{-j\beta_n x}e^{-j\beta_m z}\right) \tag{3.52}$$

$$E_{z2} = j\left(\sum_{m=-\infty}^{\infty}\sum_{n=-\infty}^{\infty}\left(\beta_{(2)}{}^2 - \beta_m{}^2\right)B_{nm}{}^{(e)}\sinh\left(\alpha_{nm}{}^{(2)}(h-y)\right)e^{-j\beta_n x}e^{-j\beta_m z}\right) \tag{3.53}$$

$$H_{x1} = -\sum_{m=-\infty}^{\infty}\sum_{n=-\infty}^{\infty}\left(\omega\varepsilon_r{}^2\varepsilon_0 A_{nm}{}^{(e)}\alpha_{nm}{}^{(1)} + jA_{nm}{}^{(h)}\beta_n\beta_m\right)\cosh(\alpha_{nm}{}^{(1)}y)e^{-j\beta_n x}e^{-j\beta_m z} \tag{3.54}$$

$$H_{x2} = \sum_{m=-\infty}^{\infty}\sum_{n=-\infty}^{\infty}\left(\omega\varepsilon_r{}^2\varepsilon_0 B_{nm}{}^{(e)}\alpha_{nm}{}^{(2)} - jB_{nm}{}^{(h)}\beta_n\beta_m\right)\cosh(\alpha_{nm}{}^{(2)}(h-y))e^{-j\beta_n x}e^{-j\beta_m z} \tag{3.55}$$

$$H_{y1} = \sum_{m=-\infty}^{\infty} \sum_{n=-\infty}^{\infty} \left(A_{nm}^{(h)} \beta_m \alpha_{nm}^{(1)} - j\omega \varepsilon_r \varepsilon_r \varepsilon_0 A_{nm}^{(e)} \beta_n \right) \sinh(\alpha_{nm}^{(1)} y) e^{-j\beta_n x} e^{-j\beta_m z} \quad (3.56)$$

$$H_{y2} = \sum_{m=-\infty}^{\infty} \sum_{n=-\infty}^{\infty} \left(j\omega \varepsilon_r^{\,2} \varepsilon_0 B_{nm}^{(e)} \beta_n - B_{nm}^{(h)} \beta_m \alpha_{nm}^{(2)} \right) \sinh(\alpha_{nm}^{(2)} (h-y)) e^{-j\beta_n x} e^{-j\beta_m z} \quad (3.57)$$

$$H_{z1} = j \left(\sum_{n=-\infty}^{\infty} \sum_{n=-\infty}^{\infty} \left(\beta_{(1)}^{\,2} - \beta_m^{\,2} \right) A_{nm}^{(h)} \cosh\left(\alpha_{nm}^{(1)} y \right) e^{-j\beta_n x} e^{-j\beta_m z} \right) \quad (3.58)$$

$$H_{z2} = j \left(\sum_{n=-\infty}^{\infty} \sum_{n=-\infty}^{\infty} \left(\beta_{(2)}^{\,2} - \beta_m^{\,2} \right) B_{nm} \cosh\left(\alpha_{nm}^{(2)} (h-y) \right) e^{-j\beta_n x} e^{-j\beta_m z} \right) \quad (3.59)$$

3.3 Boundary Conditions

Due to the symmetry of the structure with respect to the $x = 0$ plane, the symmetric (even) and anti-symmetric (odd) modes can propagate in the guide. If E_z is even or H_z in odd (similarly), a magnetic wall can be inserted at $x = 0$ without any effect on the field distribution likewise at $z = 0$. This information then allows us to consider only a quarter of the structure, i.e. treating $x = 0 \rightarrow L$ similarly to $x = 0 \rightarrow -L$ and $z = 0 \rightarrow L$ similarly to $z = 0 \rightarrow -L$. The fields at the interface $y = d$ are matched and solved for the propagation constant.

In summary the total fields derived must satisfy the boundary condition. Considering the symmetry with respect to the y-axis, we have the following four boundary conditions for the printed periodic structure [38]:

(1)	$E_{z1} = E_{z2}$	$(x,z) \in$ Unit Cell	$0 < x < L$ $0 < z < L$
(2)	$E_{x1} = E_{x2}$	$(x,z) \in$ Unit Cell	$0 < x < L$ $0 < z < L$

(3)	(a)	$E_{z1}=0$	$(x,z)\in$ Patch	$0<x<t$ $0<z<t$
	(b)	$H_{z1}=H_{z2}$	$(x,z)\in$ Aperture	$t<x<L$ $t<z<L$
(4)	(a)	$E_{x1}=0$	$(x,z)\in$ Patch	$0<x<t$ $0<z<t$
	(b)	$H_{x1}=H_{x2}$	$(x,z)\in$ Aperture	$t<x<L$ $t<z<L$

The coefficients $A_{nm}^{(e)}$, $A_{nm}^{(h)}$, $B_{nm}^{(e)}$ and $B_{nm}^{(h)}$ are unknowns; their relations can be found by applying proper boundary conditions along the air-dielectric interface. The appropriate boundary conditions are applied along the air-dielectric interface including the center conductor. It should be stated again that the superposition of the TE^z and TM^z modes must satisfy the boundary conditions along this interface. Considering the symmetry with respect to the y axis, the appropriate boundary conditions along the interface for $x>0$ that must be enforced there are four mutually independent equations are. It should be noted that the same applies for $x<0$:

$$\left.\begin{aligned}
&\sum_{m=-\infty}^{\infty}\sum_{n=-\infty}^{\infty}\overline{A_{nm}}^{(e)}\left(\beta_{(1)}{}^2-\beta_m{}^2\right)e^{-j\beta_n x}e^{-j\beta_m z}=0 && |x|<t\\
&\sum_{m=-\infty}^{\infty}\sum_{n=-\infty}^{\infty}P_{nm}(\beta_z)\overline{A_{nm}}^{(e)}e^{-j\beta_n x}e^{-j\beta_m z}+ && \\
&\qquad j\sum_{m=-\infty}^{\infty}\sum_{n=-\infty}^{\infty}T_{nm}(\beta_z)\overline{A_{nm}}^{(h)}e^{-j\beta_n x}e^{-j\beta_m z}=0 && t<|x|<L
\end{aligned}\right\}\quad(3.60a,b)$$

$$\left.\begin{aligned}
&\omega\mu_0\sum_{m=-\infty}^{\infty}\sum_{n=-\infty}^{\infty}\overline{A_{nm}}^{(h)}\alpha_{nm}{}^{(1)}e^{-j\beta_n x}e^{-j\beta_m z}+ && \\
&\qquad j\sum_{m=-\infty}^{\infty}\sum_{n=-\infty}^{\infty}\overline{A_{nm}}^{(e)}\beta_n\beta_m e^{-j\beta_n x}e^{-j\beta_m z}=0 && |x|<t\\
&\sum_{n=-\infty}^{\infty}\sum_{n=-\infty}^{\infty}W_{nm}(\beta_z)\overline{A_{nm}}^{(h)}e^{-j\beta_n x}e^{-j\beta_m z}+ && \\
&\qquad j\sum_{n=-\infty}^{\infty}\sum_{n=-\infty}^{\infty}Q_{nm}(\beta_z)\overline{A_{nm}}^{(e)}e^{-j\beta_n x}e^{-j\beta_m z}=0 && t<|x|<L
\end{aligned}\right\}\quad(3.61a,b)$$

$$\overline{A_{nm}}^{(e)} = A_{nm}{}^{(e)} \sinh\left(\alpha_{nm}{}^{(1)} d\right) \tag{3.62}$$

$$\overline{A_{nm}}^{(h)} = A_{nm}{}^{(h)} \sinh\left(\alpha_{nm}{}^{(1)} d\right) \tag{3.63}$$

$$T_{nm}(\beta_z) = \frac{\alpha_{nm}{}^{(1)}}{\alpha_{nm}{}^{(2)}} \cosh(\alpha_{nm}{}^{(2)}(h-y)) + \beta_n \beta_m \cosh(\alpha_{nm}{}^{(1)} y) \tag{3.64}$$

$$P_{nm}(\beta_z) = \left(\omega \varepsilon_r{}^2 \varepsilon_0 \frac{\left(\beta_{(1)}{}^2 - \beta_m{}^2\right)}{\left(\beta_{(2)}{}^2 - \beta_m{}^2\right)} \alpha_{nm}{}^{(2)} + \frac{(\beta_n \beta_m)^2}{\omega \mu_0 \alpha_{nm}{}^{(2)}} \frac{\left(\beta_{(2)}{}^2 - \beta_{(1)}{}^2\right)}{\left(\beta_{(2)}{}^2 - \beta_m{}^2\right)} \right) \cosh(\alpha_{nm}{}^{(2)}(h-y)) + \omega \varepsilon_r{}^2 \varepsilon_0 \alpha_{nm}{}^{(1)} \cosh(\alpha_{nm}{}^{(1)} y) \tag{3.65}$$

$$W_{nm}(\beta_z) = \left(\beta_{(1)}{}^2 - \beta_m{}^2\right) \cosh\left(\alpha_{nm}{}^{(1)} d\right) + \left(\beta_{(2)}{}^2 - \beta_m{}^2\right) \frac{\alpha_{nm}{}^{(1)}}{\alpha_{nm}{}^{(2)}} \cosh\left(\alpha_{nm}{}^{(2)}(h-d)\right) \tag{3.66}$$

$$Q_{nm}(\beta_z) = \left(\beta_{(2)}{}^2 - \beta_{(1)}{}^2\right) \frac{\beta_n \beta_m}{\omega \mu_0 \alpha_{nm}{}^{(2)}} \cosh\left(\alpha_{nm}{}^{(2)}(h-d)\right). \tag{3.67}$$

3.4 Matrix Presentation of 2-D Printed Periodic Structure

Applying the Floquet theorem for periodic structures, the 2-D structure can be considered as a unit cell and then expanded as the theorem dictates. This unit cell shown in Fig. 3-3 has been divided into nine different sections where sections A, B, C, D, F, G, H and I are the dielectric and section E is the patch.

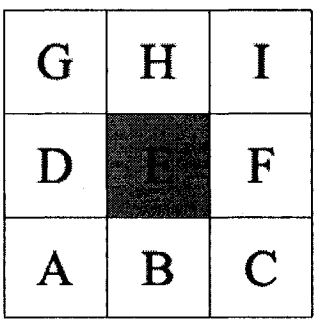

Fig. 3-3: Unit Patch

Applying the appropriate equation to the correct region, equation 3.61b and 3.62b are applied to all sections except E. Equations 3.61a and 3.62a are applied to region E. Several points along the x and z axis are taken by varying the counters n and m in $\overline{A}_{nm}^{(e)}$ and $\overline{A}_{nm}^{(h)}$. The appropriate equations are applied to the various regions. The coefficients are truncated to –N to N for both n and m. This limits the number of coefficients for $\overline{A}_{nm}^{(e)}$ and $\overline{A}_{nm}^{(h)}$ respectively to $2N + 1$. The coefficients are then arranged in a matrix form to which the singular value decomposition is applied. The smallest singular value, σ_L is then used to find the phase constant at a particular frequency.

The resulting matrix referred to as the solution matrix is outlined below in Equation 3.68.

$$\begin{matrix} \\ (1\text{-}r)(2N_z+1)/2 \text{ points on the first aperture in the z-plane} \\ r(2N_z+1) \text{ points on the patch in the z-plane} \\ (1\text{-}r)(2N_z+1)/2 \text{ points on the first aperture in the z-plane} \end{matrix} \begin{bmatrix} \overbrace{\begin{matrix} 2N_z+1 \\ \overbrace{\begin{matrix} 2N_x+1 \\ *1 \end{matrix}} \end{matrix}} & \overbrace{\begin{matrix} 2N_z+1 \\ \overbrace{\begin{matrix} 2N_x+1 \\ *2 \end{matrix}} \end{matrix}} & \overbrace{\begin{matrix} 2N_z+1 \\ \overbrace{\begin{matrix} 2N_x+1 \\ *1 \end{matrix}} \end{matrix}} \\ \begin{matrix} *1 \\ A \\ \vdots \\ \cdots \end{matrix} & \begin{matrix} *2 \\ B \\ \vdots \\ \cdots \end{matrix} & \begin{matrix} *1 \\ C \\ \vdots \\ \cdots \end{matrix} \\ \begin{matrix} *1 \\ D \\ \vdots \\ \cdots \end{matrix} & \begin{matrix} *2 \\ E \\ \vdots \\ \cdots \end{matrix} & \begin{matrix} *1 \\ F \\ \vdots \\ \cdots \end{matrix} \\ \begin{matrix} *1 \\ G \\ \vdots \end{matrix} & \begin{matrix} *2 \\ H \\ \vdots \end{matrix} & \begin{matrix} *1 \\ I \\ \vdots \end{matrix} \end{bmatrix} \begin{bmatrix} \vdots \\ \overline{A}_{mn}^{(e)} \\ \vdots \\ \overline{A}_{mn}^{(h)} \\ \vdots \\ \overline{A}_{mn}^{(e)} \\ \vdots \\ \overline{A}_{mn}^{(h)} \\ \vdots \\ \overline{A}_{mn}^{(e)} \\ \vdots \\ \overline{A}_{mn}^{(h)} \\ \vdots \end{bmatrix} = 0 \tag{3.68}$$

*1 - $\dfrac{(1-r)(2N_z+1)}{2}$ points on the first aperture in the z-plane

*2 - $\dfrac{r(2N_z+1)}{2}$ points on the patch in the z-plane.

Chapter 4

SIMULATION RESULTS

4.1 2-D MM-PM Technique Parametric Study

The performance of the MM-PM technique is tested and different program parameters are determined to generate results in an adequate amount of time. The expected result from the singular value decomposition is a curve of the smallest singular value against the propagation constant. The lowest points in the curve are further used as the solution for the homogenous equation, $A(\beta, f) = 0$. Therefore for a given frequency the lowest points of the curve correspond to the propagation constants at that frequency. Also from the parametric study for h, N and β_x it is expected that as h and N are increased and β_x is decreased the lowest points on the curves would converge to common points.

For the parametric study the following parameters are kept constant: $d = 1.27mm$, $L = 6.35mm$, $t = 0.635mm$ and $\varepsilon_r = 8.875$. Depending on the test β_x, the truncating factor N and the height of the substrate h are varied. It is important to note that the logarithm of the smallest singular value, σ_L is plotted.

4.1.1 Varying the truncating factor N

For the results depicted in Fig. 4-1, the following parameters were used: $h = 6.35mm$ and $\beta_x = 10e^{-5}$. In the Fig. 4-1, we see the result of varying N, the truncating

factor. By varying N, the smallest singular value follows similar patterns where valleys occur at the approximately the same positions. From this result it can be seen that increasing the truncation value has little effect on the solution as the valleys occur at approximately the same β_z/k_0. However, it should be noted that the main interests are where the valleys occur, this appears to be constant. Thus in the interest of processing time, the value of $N = 7$ is used since $N = 7$ and $N = 10$ were a closer match.

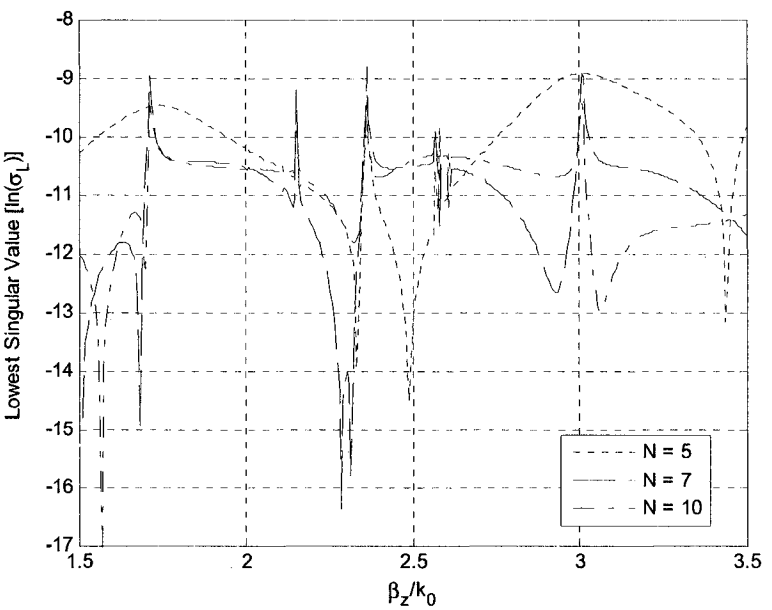

Fig. 4-1: Lowest Singular Value for different values of N

4.1.2 Varying *h*, height of the air substrate

Varying the height of the air substrate resulted in no change in the results as seen in Fig. 4-2, where major valleys occurred at 1.7 and 2.3. From this result we can conclude that by increasing the height of the air substrate to a large enough height we can simulate for an open air environment, since it has no effect on the solution.

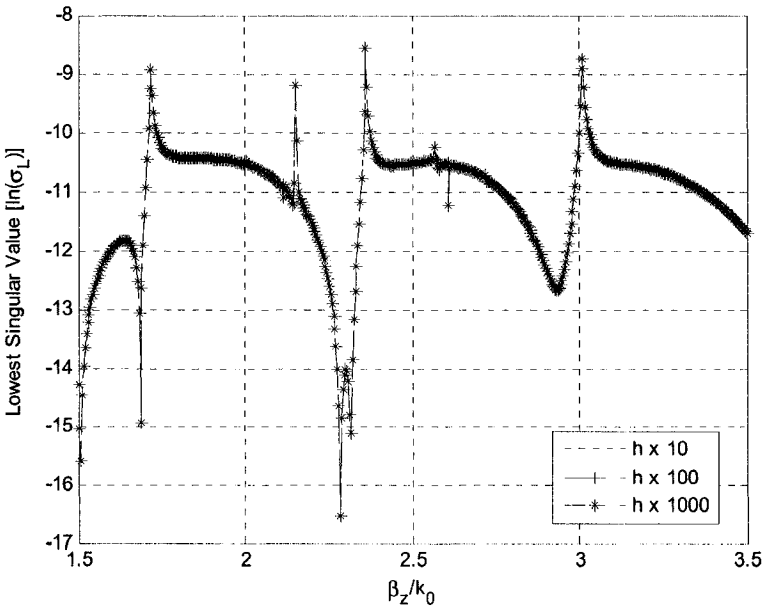

Fig. 4-2: Varying h(mm), the height of the air substrate

4.1.3 Varying β_x

From Fig. 4-3, varying β_x caused a vertical shift in the results. In all three graphs, the valleys occurred at the same place, similar to the parametric study of varying *N*. The vertical shift in the cures can be ignored since the regions of interest are the valleys which are consistent throughout the different β_x. It should be noted that as β_x gets larger the difference between the highest point and the lowest point in the curves gets smaller. Therefore to make it easier to find the lowest points β_x should be kept at approximately $10e^{-5}$ to make it easier for the algorithm to find the lowest point.

Fig. 4-5 shows several spurious responses due to the solution matrix becoming increasingly ill-conditioned. However, looking outside the spurious responses, it can be noted that there are significant areas where prominent valleys occur. For Fig. 4-5 these

areas occur approximately at $\beta_z/k_0 = 1.55, 2.4$ and 3.2. These results tell us that the dominant mode occurs at these points.

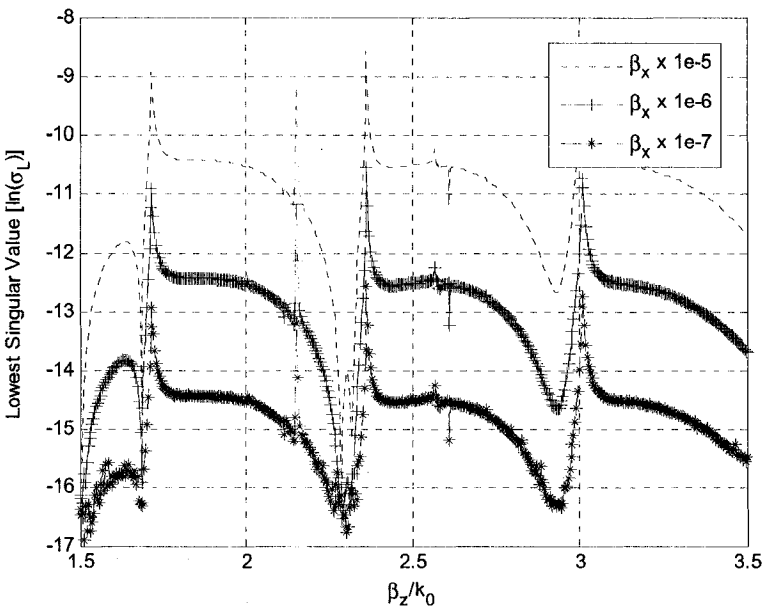

Fig. 4-3: Lowest Singular Value for different values for β_x

4.1.4 Singular Value Decomposition

In the results depicted in Fig. 4-4 to Fig. 4-5 the following parameters were used $\beta_x = 1e^{-5}$, N = 7 and h = 12.7mm. Fig. 4-4 is similar to that of Fig. 4-5 but at a different frequency. Observing the results from Fig. 4-4, we can see some spurious results. What's more looking at the general outline of the trend we can see that as before there are areas where there are valleys at particular values. In Fig. 4-4 valleys occurred approximately at $\beta_z/k_0 = 1.55, 2.3$ and 2.8.

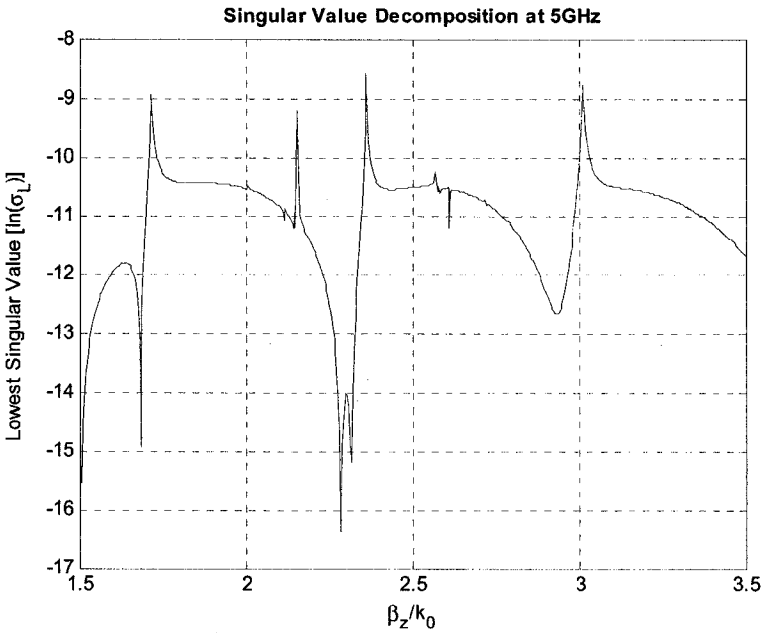

Fig. 4-4: Lowest Singular Value for frequency = 5GHz.

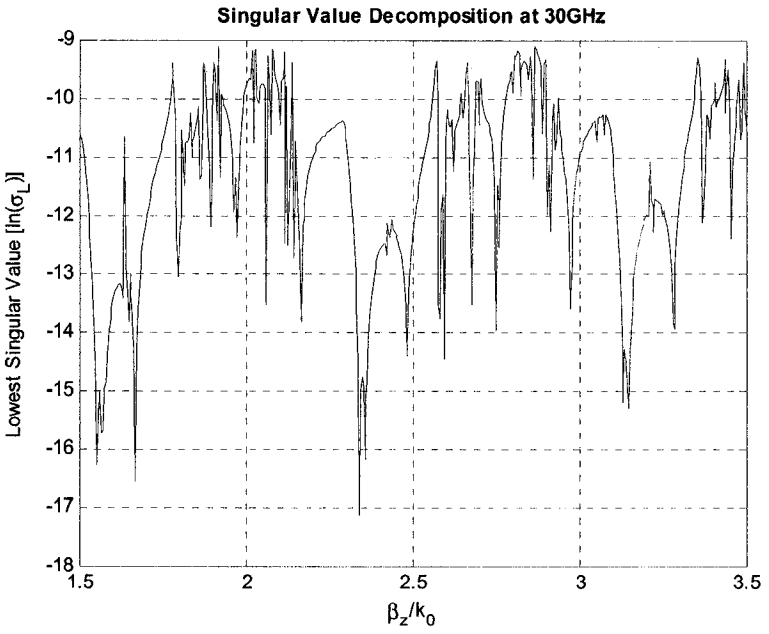

Fig. 4-5: Lowest Singular Value for frequency = 30GHz.

The results from the figures indicate that as the frequency increase more spurious results occur.

4.2 1-Dimensional Limiting Case

The 2-D MM-PM technique was applied to a 1-D case, where the patches were made as long as possible in the *z* plane. The patches were then made so that the distances were as large as possible in the *x* axis. The results from these simulations were then compared to that of the microstrip case presented by Mohebbi [6] in his work.

The structure simulated had the following parameters: L = 21mm, t = 1.27mm, d = 1.27mm, h = 127mm. These parameters are also used in 1-D MM-PM. The results from both simulations can be seen in Fig. 4-6. In this figure the results from a similar structure is simulated using HFSS.

In Fig. 4-6 it can be seen that there is a very good match between the 1-D MM-PM technique and the 2-D MM-PM method. From this, it can also be concluded that in the limiting case, the 2-D MM-PM results compare very well with the results presented by Mittra et al [38], since the 1-D MM-PM method had a good match in the results as presented by Mohebbi [6].

The HFSS results did not produce a close match to the results as shown in the figure, and as the frequency increased the difference between the graphs increased. However the results are positive since the difference in the structure can be attributed to not being an infinite structure in the *z* plane in HFSS.

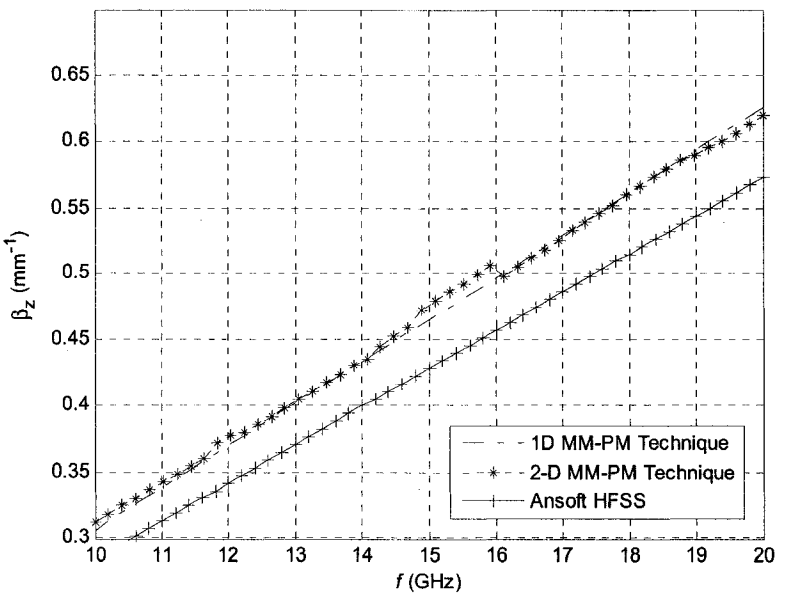

Fig. 4-6: Dispersion characteristics for 1-D structures

4.3 2-D MM-PM Technique Versus Ansoft Software

The results shown in next few figures are the calculated dispersion curve from the MM-PM technique outlined earlier and using commercial available software. Three different situations, L = 6.35mm, h = 12.7mm, t = 0.635mm, d = 1.27mm, ε_r = 8.875, L = 6.35mm, h = 12.7mm, t = 0.635mm, d = 1.27mm, ε_r = 10.2, and L = 8.5mm, h = 17.0mm, t = 0.85mm, d = 1.7mm, ε_r = 10.2, were considered, where the difference between the situation 1 and 2 was in ε_r. For situations 2 and 3 the dimensions of the patch differed. In the Matlab simulation, the following variables were set at the following values $\beta_x = 10e^{-5}$, seed value of $\beta_z / k_0 = 2.1$, $N = 7$.

Looking at Fig. 4-7, a close match between the MM-TM technique, Ansoft Designer and Ansoft HFSS can be seen. While the Ansoft software results show a linear variation of

β_z with frequency, MM-TM technique results fluctuate. However, the linear trends in both are approximately the same over the frequency range of 0 to 20GHz.

Fig. 4-8 again shows a close match between the slopes of Ansoft Designer and HFSS and the MM-PM technique curve. However, the Ansoft software curve is slightly higher than that of the MM-PM technique curve. Furthermore the difference is more evident at high frequencies.

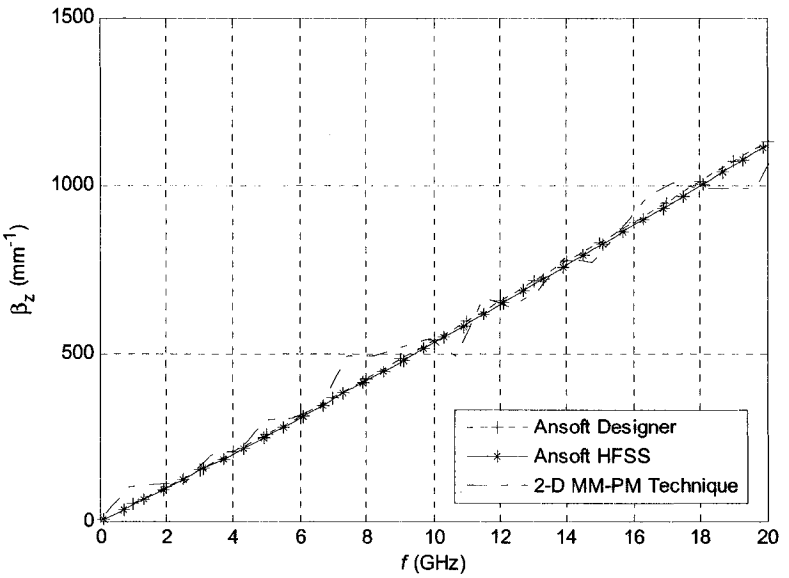

Fig. 4-7: Dispersion curve for MM-TM technique vs. Ansoft for L = 6.35mm, h = 12.7mm, t = 0.635mm, d = 1.27mm, ε_r = 8.875.

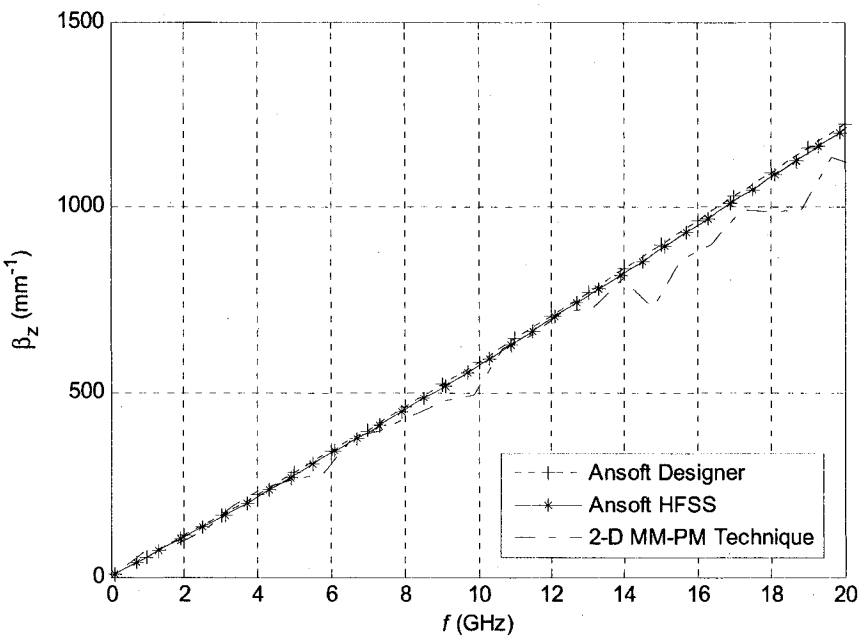

Fig. 4-8: Dispersion curve for MM-PM technique vs. Ansoft for L = 6.35mm, h = 12.7mm, t = 0.635mm, d = 1.27mm, ε_r = 10.2.

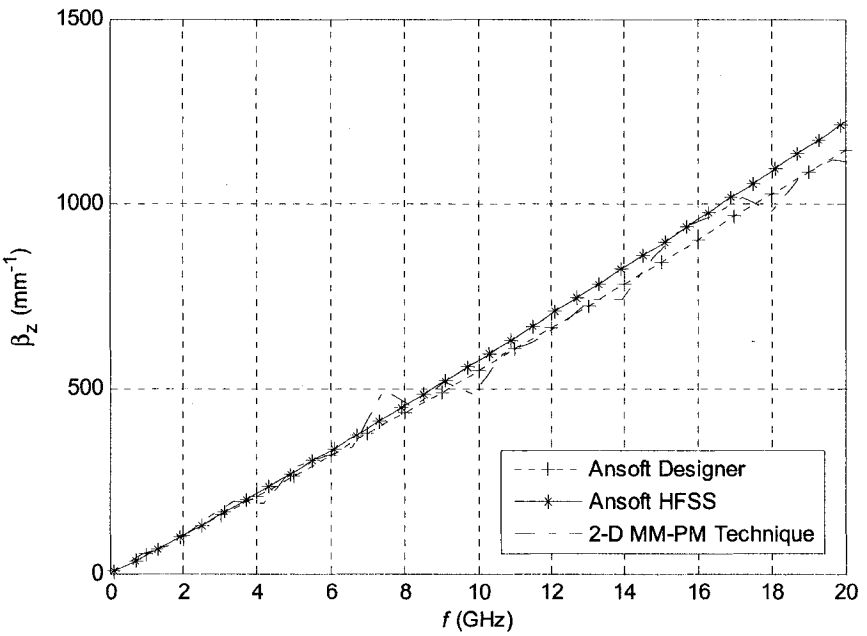

Fig. 4-9: Dispersion curve for MM-PM technique vs. Ansoft for L = 8.5mm, h = 17.0mm, t = 0.85mm, d = 1.7mm, ε_r = 10.2.

Fig. 4-9 shows an excellent match between the slope of the Ansoft Designer curve and that of the MM-PM technique curve. When compared with HFSS at low frequencies, the 2D MM-PM technique produces a good match, but as the frequency increases over approximately 8GHz the difference becomes more prominent.

4.4 A Comparison with Experimental Data

4.4.1 One- Dimensional MM-PM Technique

To determine the propagation constant to compare with the developed MM-PM technique a strip-line was built with the following properties: L = 25mm, t = 2.5mm, d = 62mil, ε = 2.2 and a depth of 15.6cm. The device can be seen in Fig. 4-10. A network analyzer was used to measure the S parameter of the structure. These results were then loaded into ADS and the optimizer feature was used to match the s- parameters to an ideal transmission line while optimizing ε_r. For this the physical length is matched to the actual length and the phase response is used to optimize. In Appendix C, the schematic of the design is shown. The results can be seen in Fig. 4-11.

A similar structure was simulated using the MM-PM technique; these results can also be seen in Fig. 4-11. It should be noted that in the MM-PM technique, the height of the air substrate needs to be defined. Thus to make the simulated situation in the MM-PM technique similar to that of the open air environment for the case of the network analyzer, the height was set to a relatively large value [6].

From the results in Fig. 4-11, it can be shown that both the MM-PM technique result and the network analyzer result provide a linear result. Furthermore we can see that there is a

very close match between the three results. It should be noted that some difference in the result is expected due to imperfections in the fabrication of the device, which are made more pronounced at high frequencies. In summary, the results show that the MM-PM technique for strip-line produced a very good approximation for the dispersion characteristics.

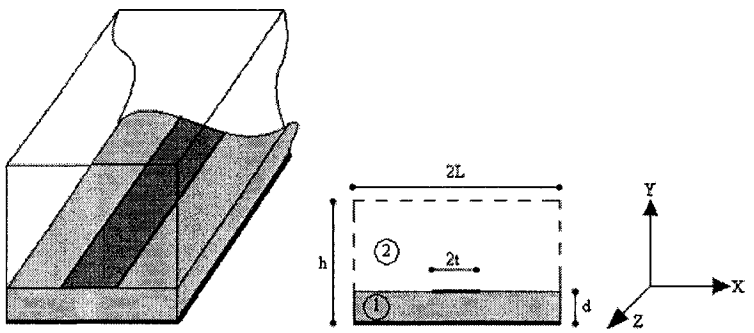

Fig. 4-10: Shielded Microstrip Line

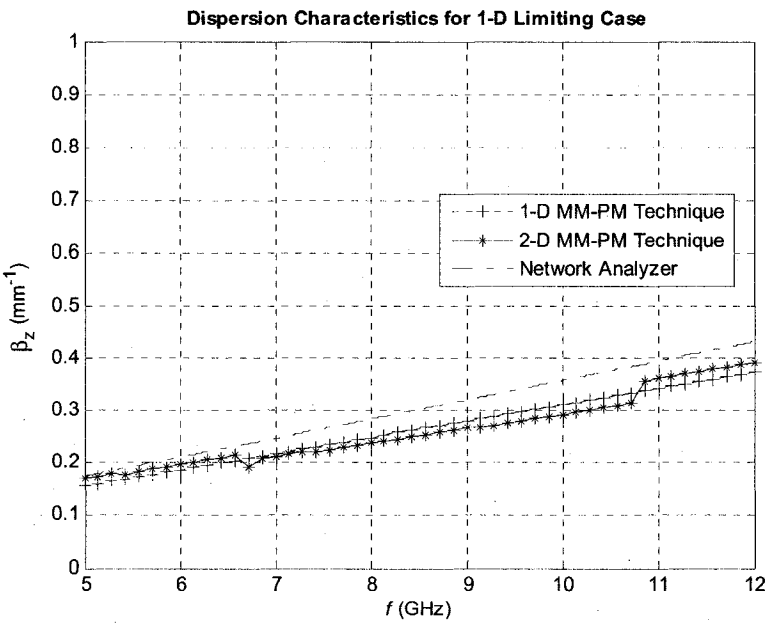

Fig. 4-11: MM-PM Technique vs. network analyzer for 1-D structure.

4.4.2 Two- Dimensional MM-PM Technique

To determine the measured phase constant of a 2-D structure, as seen in Fig. 4-12, the phase component of the $S_{1,2}$ was measured. A similar structure was then simulated using the 2D MM-PM technique method and HFSS. The results shown in Fig. 4-13 are the simulated results and the measured results for a 2-D structure with the following properties; L = 15mm, ε= 2.2, d = 62mil, t = 23mm. For the simulated results, h = 620mil used. This was to simulate the open air environment that is in the experiment.

The results show a relatively close match between the HFSS and the network analyzer results. However, both results have lower slopes that the 2-D MM-PM technique. Possible reasons for this could be less than ideal test conditions and fabrication errors. With respect to the 2D MM-PM technique it appears that as the structure gets larger the solution matrix becomes more ill-conditioned and so can produce errors. Overall the results were a good match.

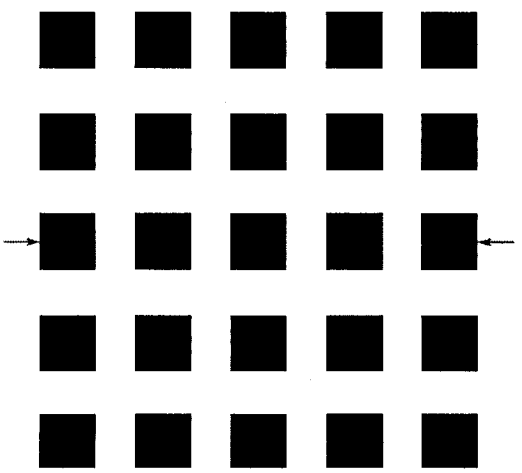

Fig. 4-12 Simulated 2-D Structure

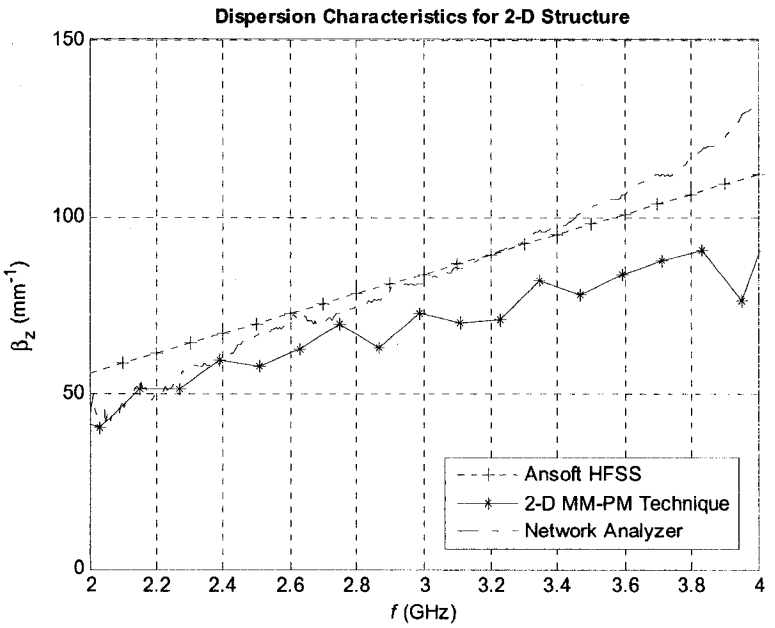

Fig. 4-13: MM-PM technique vs. network analyzer for 2-D structure

4.5 Feed Location Combinations

In the previous sections the devices were fed from the centre patches that are located at opposite ends of the devices. In this section the locations of the feeds are varied, using Ansoft HFSS, to see how it compares with that of the 2-D MM-PM technique. Two different feed combinations were used.

First, the feed points are located on patches mirrored on the y-z plane and adjacent to the centre patches as shown in Fig. 4-14. The second feed combination used is shown in Fig. 4-15. The numerical results from two different devices and for the two configurations are shown in Fig. 4-16 and Fig. 4-17. From Fig. 4-16, at low frequencies it is seen that the two different feed styles match the MM-PM technique. As the frequency increases the first feed style results deviate from the results of the second feed style and that of the

MM-PM technique. For the second device this is not the case. Three results in Fig. 4-17 are approximately the same.

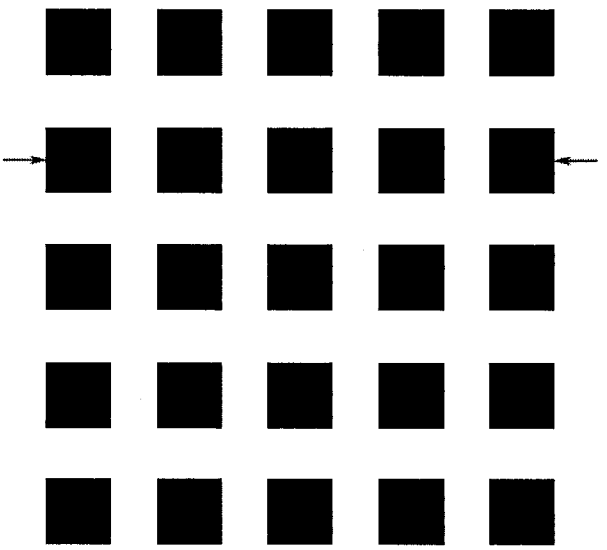

Fig. 4-14 Feed style 1.

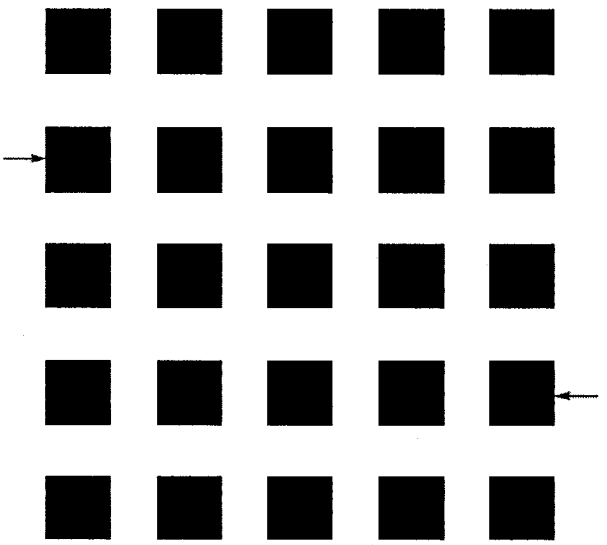

Fig. 4-15 Feed style 2.

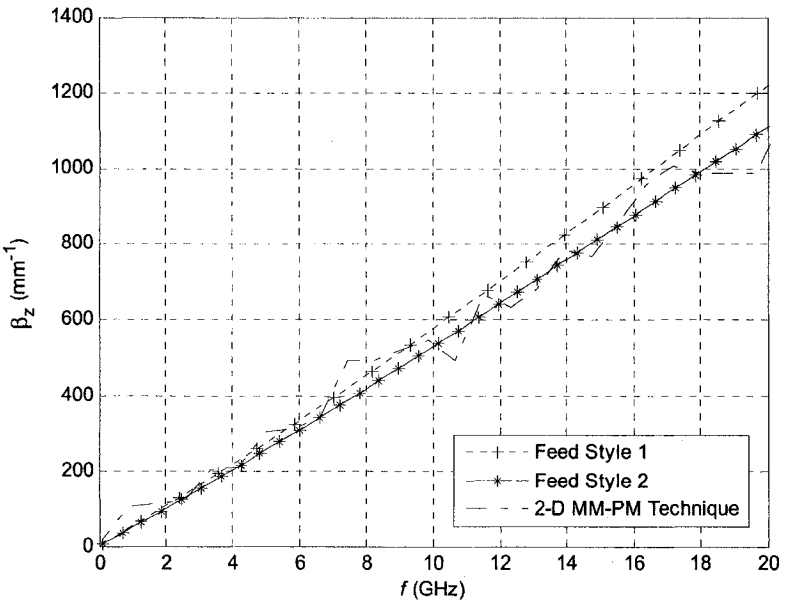

Fig. 4-16 Dispersion curve Feed style for L = 6.35mm, h = 12.7mm, t = 0.635mm, d = 1.27mm, ε_r = 8.875.

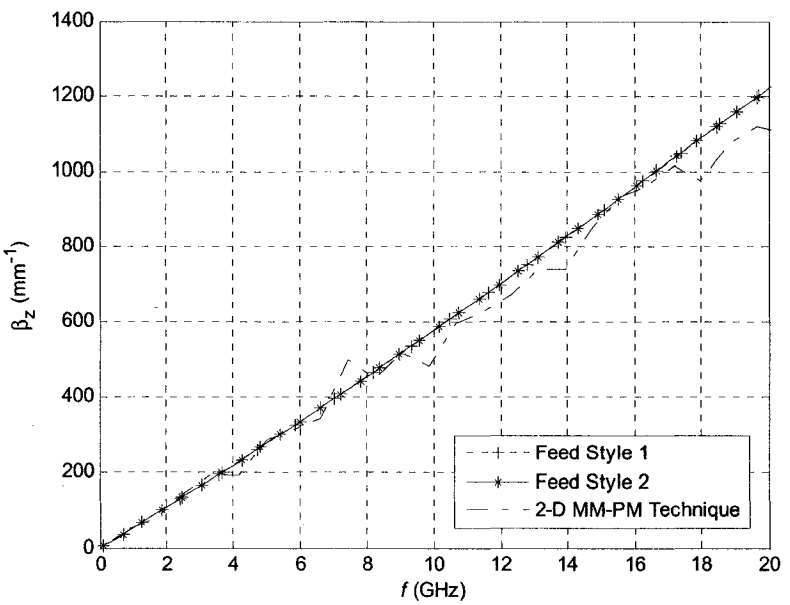

Fig. 4-17 Dispersion curve Feed style for L = 8.5mm, h = 17.0mm, t = 0.85mm, d = 1.7mm, ε_r = 10.2.

Chapter 5

CONCLUSION

In this thesis we adopted the hybrid method of the mode matching technique and develop it to calculate the dispersion characteristics of a 2-D periodic structure. In the MM-PM technique an infinite number of periodic patches were distributed on a substrate. We assumed that the strips are infinitely small and a perfect metallic shield is placed at a large distance above the patches to prevent radiation. Floquet's theorem is used to obtain the field equations both in the air and in the dielectric substrate. Then by imposing boundary conditions at the interface of the air and substrate, a set of equations are obtained. These equations are expressed in a matrix form and then solved to yield the dispersion characteristics.

There is a close match of the results of the 2-D MM-PM technique developed and the results generated using HFSS, Ansoft Designer and the limiting case for the 1-D MM-PM method, as seen Fig. 4-6 to Fig. 4-9. A reasonable match between the 2-D structure and the 2-D MM-PM technique is also obtained. Likewise there is a good match between the experimental results, Fig. 4-11 and Fig. 4-12, for the 1-D and 2-D structure and the MM-PM technique. The implications of these results are that the MM-PM technique is valid alternative method to calculate the dispersion characteristics.

The parametric study showed that several modes appeared since several valleys in Fig. 4-1 to Fig. 4-5 were observed. It should be noted that the spurious valleys present in the

results indicated that the solution matrix was ill-conditioned. These results are more significant when a large structure is under test, since for large structures large values are included in the solution matrix and these further cause large variations in the elements' values of the matrix.

It is noted from the experimental data for 1-D and 2-D periodic structure that the 2-D MM-PM technique worked best at lower frequencies. This is expected since like before large frequency values increased the condition of the matrix making it more difficult to extract the propagation constant. Therefore with a small structure care was taken in choosing the parameters used. The SVD is powerful enough tool to compensate for small departures and provide reasonable results.

It was noticed from the experimental data for 1-D and 2-D periodic structures that the 2-D MM-PM, technique worked best at lower frequencies. This is expected since large frequency values increased the condition of the matrix, making it more difficult to extract the propagation constant.

It was seen that changes to the dimension of the metal patch brought negligible changes in the dispersion characteristics. However changes in ε_r did bring noticeable changes to the dispersion characteristics. This is seen in both the theoretical results and simulated results. These results confirm that ε_r does in fact have a larger effect on the dispersion characteristics.

In summary it has been shown that the MM-PM technique can be successfully applied to calculate the dispersion characteristics for the 2-D periodic structure, with good accuracy

as shown by comparison with results from commercially available sofware and also with experimental results.

5.1 Further Work

The current work was developed for a simple shaped patch arranged in an array format. Further work could be done on the design of some other shapes such as circular patches.

Extending this work to 3-D structures is another possibility for further work. But again, care need to be taken as the matrices could be very ill conditioned. In pursuing this avenue of work, efforts would need to be put into improving the conditioning of the matrices before solving them.

Currently there is a lot of work being done in designing 2-D periodic structures by having a patterned ground plane which is separated from a microstrip line by a dielectric substrate. Therefore this work could be developed to look at having a patterned ground plane as opposed to a simple sheet as ground.

The propagation constant β in this work was considered to be a scalar and real quantity. As stated in Scarmozzino et al. [7], this would provide results of interest but may not be accurate in determining the propagation constant. This could also be used to explain why the experimental results obtained from measurements compared to that obtained from the MM-PM method do not match. An improvement to the results could be achieved by considering the case where the propagation constant is complex ($\alpha + j\beta$). This would give us a better understanding of the band-gap for the structure under investigation.

REFERENCES

[1] **S.K. Parui and S. Das;** A SIMPLE ELECTROMAGNETIC BANDGAP STRUCTURE FOR MICROSTRIP LINE; *Indian Institute Of Technology, Kharagpur 721302*, December 20-22,2004 pp.547-8

[2] **C. C. Chang, Y. Qian and T. Itoh;** ANALYSIS AND APPLICATIONS OF UNIPLANAR COMPACT PHOTONIC BAND-GAP STRUCTURES. *PIER.* 2003, Vols. 41, pp.211–235.

[3] **F.R. Yang, K.P. Ma, Y. Qian, T. Itoh;** A UNIPLANAR COMPACT PHOTONIC-BAND-GAP (UC-PBG) STRUCTURE AND ITS APPLICATIONS FOR MICROWAVE CIRCUITS. *IEEE Transactions On Microwave Theory And Techniques.* 1999, Vol. 47, p.8.

[4] **F.R. Yang, R. Coccioli and Y. Qian;** PLANAR PBG STRUCTURES: BASIC PROPERTIES AND APPLICATIONS. *IEICE Trans. Electron.* 2000, Vol. E, p.5.

[5] **S.G. Johnson and J. D. Joannopoulos;** INTRODUCTION TO PHOTONIC CRYSTALS: BLOCH'S THEOREM, BAND DIAGRAMS, AND GAPS (BUT NO DEFECTS). *Massachusetts Institute of Technology.* 3rd, 2003.

[6] **H.R. Mohebbi;** (2006) MODE MATCHING TECHNIQUE FOR CALCULATING THE DISPERSION CURVE OF ONE-DIMENSIONAL PERIODIC STRUCTURES. *Masters Thesis,* Concordia University

[7] **R. Scarmozzino, A. Gopinath, R. Pregla,and S. Helfert;** NUMERICAL TECHNIQUES FOR MODELING GUIDED-WAVE PHOTONIC DEVICES. *IEEE Journal Of Selected Topics In Quantum Electronics.* 2000, Vol. 6, p.1.

[8] **T. Itoh;** PLANAR TRANSMISSION LINE STRUCTURES, *IEEE Press*, 1987.

[9] **L. Young, and H. Sobol;** ADVANCES IN MICROWAVES, vol. 8, *Academic Press*, 1966.

[10] **A.S. Omar and K. Schunemann;** - FORMULATION OF THE SINGULAR INTEGRAL EQUATION TECHNIQUE FOR PLANAR TRANSMISSION LINES - *IEEE Transactions on Microwave Theory and Techniques*, Vol. Mtt-33 , No, 12, December 1985 pp. 1313 - 1322

[11] **E. Yamashita and K. Atsuki;** ANALYSIS OF MICROSTRIP-LIKE TRANSMISSION LINES BY NONUNIFORM DISCRETIZATION OF INTEGRAL EQUATIONS, *IEEE Transactions on Microwave Theory and Techniques*, 1976, pp. 195 - 200

[12] **T. Itoh and R. Mittra;** SPECTRAL-DOMAIN APPROACH FOR CALCULATING THE DISPERSION CHARACTERISTICS OF MICROSTRIP LINES, *IEEE Transactions on Microwave Theory and Techniques,* 1973 pp. 496 - 499

[13] **A.C. Cangellaris;** - NUMERICAL STABILITY AND NUMERICAL DISPERSION OF A COMPACT 2-D/FDTD METHOD USED FOR THE DISPERSION ANALYSIS OF WAVEGUIDES, *Microwave And Guided Wave Letters*, Vol. 3, No. 1, January 1993, pp. 3 - 5

[14] **S.Ju, H. Kim and H.H. Kim;** - A STUDY OF THE NUMERICAL DISPERSION RELATION FOR THE 2-D ADI-FDTD METHOD *IEEE; Microwave And Wireless Components Letters*, Vol. 13, No. 9, September 2003, pp. 405 - 407

[15] Manuals for Ansoft HFSS and Ansoft Designer, version 9, www.ansoft.com, 2005.

[16] **R Mullen and T. Belytschko;** - DISPERSION ANALYSIS OF FINITE ELEMENT WAVE EQUATION - *International Journal For Numerical Methods In Engineering*, 1982 - doi.wiley.com, pp. 11 - 29

[17] **K.S. Yee;** NUMERICAL SOLUTION OF INITIAL BOUNDARY VALUE PROBLEMS INVOLVING MAXWELL'S EQUATIONS IN ISOTROPIC MEDIA; *IEEE Transactions on Antennas And Propagation* Vol. Ap-14, No. 3 May, 1966, pp. 302 - 307

[18] **K.S. Kunz and R.J. Luebbers;** THE FINITE DIFFERENCE TIME DOMAIN METHOD FOR ELECTROMAGNETIC; *Boca Raton*: CRC Press, c1993

[19] **J .P. Webb;** APPLICATION OF THE FINITE-ELEMENT METHOD TO ELECTROMAGNETIC AND ELECTRICAL TOPICS; *Reports on Progress in Physics* 58; 1995; pp. 1673-1712

[20] **X.Q. Sheng, E.K.N. Yung, C.H. Chan;** AN EFFICIENT ANALYSIS OF MICROSTRIP LINES ON ARTIFICIAL PERIODIC STRUCTURES; *Microwave Conference*, 2000; pp. 404-407.

[21] **U. Rogge and R. Pregla;** METHOD OF LINES FOR THE ANALYSIS OF STRIP-LOADED OPTICAL WAVEGUIDES; *Journal of the Optical Society of America B*: Optical Physics, Volume 8, Issue 2, February 1991, pp.459-463

[22] **U. Rogge and R. Pregla;** METHOD OF LINES FOR THE ANALYSIS OF DIELECTRIC WAVEGUIDES; *Journal of Lightwave Technology*, Vol. 11, No. 12, December 1993; pp. 2015-9

[23] **Habib Ammari Gang Bao and Aihua W. Wood;** AN INTEGRAL EQUATION METHOD FOR THE ELECTROMAGNETIC SCATTERING FROM CAVITIES; *Mathematical Methods in the Applied Sciences*; Volume 23, Issue 12, 7 Jul 2000; pp.1057 – 1072

[24] **T. Itoh;** A TECHNIQUE FOR COMPUTING DISPERSION CHARACTERISTICS OF SHIELDED MICROSTRIP LINES; *IEEE Transactions on Microwave Theory and Techniques*, October 1974; pp. 896 - 898

[25] **T. Itoh And R. M. Ittra;** SPECTRAL-DOMAIN APPROACH FOR CALCULATING THE DISPERSION CHARACTERISTICS OF MICROSTRIP LINES; *IEEE Transactions on Microwave Theory and Techniques*, July 1973; pp. 496 - 499

[26] **R. Mittra, Hou Yun-Li and V. Jamnejad;** ANALYSIS OF OPEN DIELECTRIC WAVEGUIDES USING MODE-MATCHING TECHNIQUE AND VARIATIONAL METHODS., s.l. : *IEEE Transactions On Microwave Theory and Techniques*, Jan 1980, pp. 36 - 43

[27] **R.Lee and S. W.Mittra;** ANALYTICAL TECHNIQUES IN THE THEORY OF GUIDED WAVES. *New York : MacMillan*, 1971

[28] **S. Liguo, and X. Shanjia;** A SIMPLE AND ACCURATE METHOD FOR ANALYSIS OF DIELECTRIC PERIODIC STRUCTURES. 10,: *International Journal of Infared and Millimeter Waves,* Oct 1992, Vol. 13; pp. 1667-1676

[29] **R. E Collin;** FOUNDATION FOR MICROWAVE ENGINEERING; McGraw-Hill Book Company, 1992.

[30] **S.C. Chapra, and R.P. Canale.** NUMERICAL METHODS FOR ENGINEERS. 2nd Ed. *McGraw Hill*, New York, 1988.

[31] **L. Matekovits, Th. Bertuch and M. Orefice;** SOLUTION BY SVD OF ILL-CONDITIONED MATRIX EQUATIONS IN PERIODIC STRUCTURE ANALYSIS. *IEEE Antennas and Propagation Society International Symposium.* 2006; pp. 4623 - 4626

[32] **Li Er Ping and Ahmed Shahid;** APPLICATION OF SINGULAR VALUE DECOMPOSITION ON FDTD SIMULATION RESULT - A NOVEL APPROACH FOR MODAL ANALYSIS OF COMPLEX ELECTROMAGNETIC PROBLEMS. *IEEE Microwave And Wireless Components Letters.* 2007, Vol. 14, 11.; pp. 519- 521

[33] **V.A. Labay and J. Bornemann;** MATRIX SINGULAR VALUE DECOMPOSITION FOR POLE-FREE SOLUTIONS OF HOMOGENEOUS MATRIX EQUATIONS AS APPLIED TO NUMERICAL MODELING METHODS. *IEEE Microwave and Guided wave Letters.* 1992, Vol. 2, Issue 2; pp. 49-51

[34] **Tianxia Zhao, D.R. Jackson, J.T. Williams, H.Y. D. Yang and A.A. Oliner;** 2-D PERIODIC LEAKY-WAVE ANTENNAS—PART I: METAL PATCH DESIGN; *IEEE Transactions on Antennas and Propagation*, Vol. 53, No. 11, November 2005 pp. 3505 - 3514

[35] **G. Lovat, P. Burghignoli and D.R. Jackson;** FUNDAMENTAL PROPERTIES AND OPTIMIZATION OF BROADSIDE RADIATION FROM UNIFORM LEAKY-WAVE ANTENNAS; *IEEE Transactions on Antennas and Propagation*, Volume 54, Issue 5, May 2006 pp.1442 – 1452

[36] **P. Baccarelli, P. Burghignoli, C. Di Nallo, F. Frezza, A. Galli, P. Lampariello, and G. Ruggieri;** FULL-WAVE ANALYSIS OF PRINTED LEAKY-WAVE PHASED ARRAYS; *International Journal of RF and Microwave Computer-Aided Engineering*; Volume 12, Issue 3 ; pp. 272 – 287

[37] **Zhao Tianxia, D.R. Jackson, J.T. Williams and A.A. Oliner;** GENERAL FORMULAS FOR A 2D LEAKY-WAVE ANTENNA; *IEEE Antennas and Propagation Society International Symposium*, 2003. pp. 1134 - 1137

[38] **R. Mittra and T. Itoh;** A NEW TECHNIQUE FOR THE ANALYSIS OF THE DISPERSION CHARACTERISTICS OF MICROSTRIP LINES. *IEEE Transactions on Microwave Theory and Techniques.;* Volume 19, Issue 1, Jan 1971 pp. 47 - 56

[39] **Constantine A. Balanis;** ADVANCED ENGINEERING ELECTROMAGNETICS.; 1938; New York; Wiley; C1989.

[40] **Constantine A. Balanis;** ANTENNA THEORY: ANALYSIS AND DESIGN.; New Jersey: John Wiley, C2005. 3rd Ed.

Appendix A

MATHEMATICAL FORMULATION

A.1. Condition 1

$$E_{z1} = -j\frac{1}{\omega\mu\varepsilon}\left(\sum_{m=-\infty}^{\infty}\sum_{n=-\infty}^{\infty}\left(\beta_{(1)}{}^2 - \beta_m{}^2\right)A_{nm}{}^{(e)}\sinh\left(\alpha_{nm}{}^{(1)}d\right)e^{-j\beta_n x}e^{-j\beta_m z}\right) \tag{A1-1}$$

$$E_{z2} = -j\frac{1}{\omega\mu\varepsilon}\left(\sum_{m=-\infty}^{\infty}\sum_{n=-\infty}^{\infty}\left(\beta_{(2)}{}^2 - \beta_m{}^2\right)B_{nm}{}^{(e)}\sinh\left(\alpha_{nm}{}^{(2)}(h-d)\right)e^{-j\beta_n x}e^{-j\beta_m z}\right) \tag{A1-2}$$

$$E_{z1} = E_{z2} \tag{A1-3}$$

$$j\left(\sum_{m=-\infty}^{\infty}\sum_{n=-\infty}^{\infty}\left(\beta_{(1)}{}^2 - \beta_m{}^2\right)A_{nm}{}^{(e)}\sinh\left(\alpha_{nm}{}^{(1)}y\right)e^{-j\beta_n x}e^{-j\beta_m z}\right) = j\left(\sum_{m=-\infty}^{\infty}\sum_{n=-\infty}^{\infty}\left(\beta_{(2)}{}^2 - \beta_m{}^2\right)B_{nm}{}^{(e)}\sinh\left(\alpha_{nm}{}^{(2)}(h-y)\right)e^{-j\beta_n x}e^{-j\beta_m z}\right) \tag{A1-4}$$

$$\sum_{m=-\infty}^{\infty}\sum_{n=-\infty}^{\infty}\left(\beta_{(1)}{}^2 - \beta_m{}^2\right)A_{nm}{}^{(e)}\sinh\left(\alpha_{nm}{}^{(1)}y\right)e^{-j\beta_n x}e^{-j\beta_m z} = \sum_{m=-\infty}^{\infty}\sum_{n=-\infty}^{\infty}\left(\beta_{(2)}{}^2 - \beta_m{}^2\right)B_{nm}{}^{(e)}\sinh\left(\alpha_{nm}{}^{(2)}(h-y)\right)e^{-j\beta_n x}e^{-j\beta_m z} \tag{A1-5}$$

Set of $\left\{e^{-j\beta_n x}\right\}$ and $\left\{e^{-j\beta_m z}\right\}$ with $\beta_n = \beta_x + \frac{2\pi n}{2L}$ and $\beta_m = \beta_z + \frac{2\pi z}{2L}$ are a complete orthogonal set over the interval of $-L < x < L$ and $-L < z < L$ therefore

$$\left(\beta_{(1)}{}^2 - \beta_m{}^2\right)A_{nm}{}^{(e)}\sinh\left(\alpha_{nm}{}^{(1)}d\right) = \left(\beta_{(2)}{}^2 - \beta_m{}^2\right)B_{nm}{}^{(e)}\sinh\left(\alpha_{nm}{}^{(2)}(h-d)\right) \tag{A1-6}$$

$$B_{nm}{}^{(e)} = A_{nm}{}^{(e)}\frac{\left(\beta_{(1)}{}^2 - \beta_m{}^2\right)}{\left(\beta_{(2)}{}^2 - \beta_m{}^2\right)}\frac{\sinh\left(\alpha_{nm}{}^{(1)}d\right)}{\sinh\left(\alpha_{nm}{}^{(2)}(h-d)\right)} \tag{A1-7}$$

A.2. Condition 2

$$E_{x1} = E_{x2} \tag{A1-8}$$

$$\sum_{m=-\infty}^{\infty}\sum_{n=-\infty}^{\infty}\left(\omega\mu_0 A_{nm}^{(h)}\alpha_{nm}^{(1)} - jA_{nm}^{(e)}\beta_n\beta_m\right)\sinh(\alpha_{nm}^{(1)}y)e^{-j\beta_n x}e^{-j\beta_m z} = \tag{A1-9}$$
$$-\sum_{m=-\infty}^{\infty}\sum_{n=-\infty}^{\infty}\left(jB_{nm}^{(e)}\beta_n\beta_m + \omega\mu_0 B_{nm}^{(h)}\alpha_{nm}^{(2)}\right)\sinh(\alpha_{nm}^{(2)}(h-y))e^{-j\beta_n x}e^{-j\beta_m z}$$

$$\left(\omega\mu_0 A_{nm}^{(h)}\alpha_{nm}^{(1)} - jA_{nm}^{(e)}\beta_n\beta_m\right)\sinh(\alpha_{nm}^{(1)}y) = \tag{A1-10}$$
$$-\left(jB_{nm}^{(e)}\beta_n\beta_m + \omega\mu_0 B_{nm}^{(h)}\alpha_{nm}^{(2)}\right)\sinh(\alpha_{nm}^{(2)}(h-y))$$

$$\left(\omega\mu_0 A_{nm}^{(h)}\alpha_{nm}^{(1)} - jA_{nm}^{(e)}\beta_n\beta_m\right)\frac{\sinh(\alpha_{nm}^{(1)}y)}{\sinh(\alpha_{nm}^{(2)}(h-y))} = \tag{A1-11}$$
$$-jB_{nm}^{(e)}\beta_n\beta_m - \omega\mu_0 B_{nm}^{(h)}\alpha_{nm}^{(2)}$$

$$\left(\omega\mu_0 A_{nm}^{(h)}\alpha_{nm}^{(1)} - jA_{nm}^{(e)}\beta_n\beta_m\right)\frac{\sinh(\alpha_{nm}^{(1)}y)}{\sinh(\alpha_{nm}^{(2)}(h-y))} = \tag{A1-12}$$
$$-jA_{nm}^{(e)}\frac{\left(\beta_{(1)}^{\ 2}-\beta_m^{\ 2}\right)}{\left(\beta_{(2)}^{\ 2}-\beta_m^{\ 2}\right)}\frac{\sinh\left(\alpha_{nm}^{(1)}d\right)}{\sinh\left(\alpha_{nm}^{(2)}(h-d)\right)}\beta_n\beta_m - \omega\mu_0 B_{nm}^{(h)}\alpha_{nm}^{(2)}$$

$$\omega\mu_0 B_{nm}^{(h)}\alpha_{nm}^{(2)} =$$
$$\left(jA_{nm}^{(e)}\beta_n\beta_m - \omega\mu_0 A_{nm}^{(h)}\alpha_{nm}^{(1)} - jA_{nm}^{(e)}\beta_n\beta_m\frac{\left(\beta_{(1)}^{\ 2}-\beta_m^{\ 2}\right)}{\left(\beta_{(2)}^{\ 2}-\beta_m^{\ 2}\right)}\right)\frac{\sinh\left(\alpha_{nm}^{(1)}d\right)}{\sinh\left(\alpha_{nm}^{(2)}(h-d)\right)} \tag{A1-13}$$

$$B_{nm}^{(h)} =$$
$$\left(\frac{jA_{nm}^{(e)}\beta_n\beta_m}{\omega\mu_0\alpha_{nm}^{(2)}} - A_{nm}^{(h)}\frac{\alpha_{nm}^{(1)}}{\alpha_{nm}^{(2)}} - \frac{jA_{nm}^{(e)}\beta_n\beta_m}{\omega\mu_0\alpha_{nm}^{(2)}}\frac{\left(\beta_{(1)}^{\ 2}-\beta_m^{\ 2}\right)}{\left(\beta_{(2)}^{\ 2}-\beta_m^{\ 2}\right)}\right)\frac{\sinh\left(\alpha_{nm}^{(1)}d\right)}{\sinh\left(\alpha_{nm}^{(2)}(h-d)\right)} \tag{A1-14}$$

$$B_{nm}^{(h)} = \left(\frac{j\beta_n\beta_m}{\omega\mu_0\alpha_{nm}^{(2)}}\frac{\left(\beta_{(2)}^{\ 2}-\beta_{(1)}^{\ 2}\right)}{\left(\beta_{(2)}^{\ 2}-\beta_m^{\ 2}\right)}A_{nm}^{(e)} - \frac{\alpha_{nm}^{(1)}}{\alpha_{nm}^{(2)}}A_{nm}^{(h)}\right)\frac{\sinh\left(\alpha_{nm}^{(1)}d\right)}{\sinh\left(\alpha_{nm}^{(2)}(h-d)\right)} \tag{A1-15}$$

A.3. Condition 3 (a)

$$E_{z1} = 0 \tag{A1-16}$$

$$E_{z1} = -j\frac{1}{\omega\mu\varepsilon}\sum_{m=-\infty}^{\infty}\sum_{n=-\infty}^{\infty}\left(\beta_{(1)}^{\ 2}-\beta_m^{\ 2}\right)A_{nm}^{(e)}\sinh\left(\alpha_{nm}^{(1)}d\right)e^{-j\beta_n x}e^{-j\beta_m z} = 0 \tag{A1-17}$$

$$\sum_{m=-\infty}^{\infty}\sum_{n=-\infty}^{\infty}\left(\beta_{(1)}^{\ 2}-\beta_m^{\ 2}\right)A_{nm}^{(e)}\sinh\left(\alpha_{nm}^{(1)}d\right)e^{-j\beta_n x}e^{-j\beta_m z} = 0 \tag{A1-18}$$

$$\sum_{m=-\infty}^{\infty}\sum_{n=-\infty}^{\infty}\overline{A_{nm}}^{(e)}\left(\beta_{(1)}^{\ 2}-\beta_m^{\ 2}\right)e^{-j\beta_n x}e^{-j\beta_m z} = 0 \tag{A1-19}$$

$$\overline{A_{nm}}^{(e)} = A_{nm}^{(e)}\sinh\left(\alpha_{nm}^{(1)}d\right) \tag{A1-20}$$

A.4. Condition 3 (b)

$$H_{x1} = H_{x2} \tag{A1-21}$$

$$\mathrm{M} = \cosh(\alpha_{nm}{}^{(2)}(h-y))e^{-j\beta_n x}e^{-j\beta_m z}$$

$$\mathrm{N} = \cosh(\alpha_{nm}{}^{(1)}y)e^{-j\beta_n x}e^{-j\beta_m z} \tag{A1-22a, b}$$

$$\sum_{m=-\infty}^{\infty}\sum_{n=-\infty}^{\infty}\left(-\omega\varepsilon_1 A_{nm}{}^{(e)}\alpha_{nm}{}^{(1)} - jA_{nm}{}^{(h)}\beta_n\beta_m\right)\cosh(\alpha_{nm}{}^{(1)}y)e^{-j\beta_n x}e^{-j\beta_m z} =$$
$$\sum_{m=-\infty}^{\infty}\sum_{n=-\infty}^{\infty}\left(\omega\varepsilon_0 B_{nm}{}^{(e)}\alpha_{nm}{}^{(2)} - jB_{nm}{}^{(h)}\beta_n\beta_m\right)\cosh(\alpha_{nm}{}^{(2)}(h-y))e^{-j\beta_n x}e^{-j\beta_m z} \tag{A1-23}$$

$$\sum_{m=-\infty}^{\infty}\sum_{n=-\infty}^{\infty}\left(-\omega\varepsilon_1 A_{nm}{}^{(e)}\alpha_{nm}{}^{(1)} - jA_{nm}{}^{(h)}\beta_n\beta_m\right)\times\mathrm{N} =$$
$$\sum_{m=-\infty}^{\infty}\sum_{n=-\infty}^{\infty}\left(\begin{array}{l}\omega\varepsilon_0 A_{nm}{}^{(e)}\dfrac{\left(\beta_{(1)}{}^2-\beta_m{}^2\right)}{\left(\beta_{(2)}{}^2-\beta_m{}^2\right)}\alpha_{nm}{}^{(2)} - \\ \quad j\left(\dfrac{j\beta_n\beta_m}{\omega\mu_0\alpha_{nm}{}^{(2)}}\dfrac{\left(\beta_{(2)}{}^2-\beta_{(1)}{}^2\right)}{\left(\beta_{(2)}{}^2-\beta_m{}^2\right)}A_{nm}{}^{(e)} - \dfrac{\alpha_{nm}{}^{(1)}}{\alpha_{nm}{}^{(2)}}A_{nm}{}^{(h)}\right)\beta_n\beta_m\end{array}\right)\times\frac{\sinh\left(\alpha_{nm}{}^{(1)}d\right)}{\sinh\left(\alpha_{nm}{}^{(2)}(h-d)\right)}\times\mathrm{M} \tag{A1-24}$$

$$\sum_{m=-\infty}^{\infty}\sum_{n=-\infty}^{\infty}\left(-\omega\varepsilon_1 A_{nm}{}^{(e)}\alpha_{nm}{}^{(1)} - jA_{nm}{}^{(h)}\beta_n\beta_m\right)\times\mathrm{N} =$$
$$\sum_{m=-\infty}^{\infty}\sum_{n=-\infty}^{\infty}\left(\begin{array}{l}\omega\varepsilon_0 A_{nm}{}^{(e)}\dfrac{\left(\beta_{(1)}{}^2-\beta_m{}^2\right)}{\left(\beta_{(2)}{}^2-\beta_m{}^2\right)}\alpha_{nm}{}^{(2)} \\ \quad + \dfrac{(\beta_n\beta_m)^2}{\omega\mu_0\alpha_{nm}{}^{(2)}}\dfrac{\left(\beta_{(2)}{}^2-\beta_{(1)}{}^2\right)}{\left(\beta_{(2)}{}^2-\beta_m{}^2\right)}A_{nm}{}^{(e)} \\ \quad + j\dfrac{\alpha_{nm}{}^{(1)}}{\alpha_{nm}{}^{(2)}}A_{nm}{}^{(h)}\beta_n\beta_m\end{array}\right)\times\frac{\sinh\left(\alpha_{nm}{}^{(1)}d\right)}{\sinh\left(\alpha_{nm}{}^{(2)}(h-d)\right)}\times\mathrm{M} \tag{A1-25}$$

$$\sum_{m=-\infty}^{\infty}\sum_{n=-\infty}^{\infty}\left(-\omega\varepsilon_1 A_{nm}^{(e)}\alpha_{nm}^{(1)} - jA_{nm}^{(h)}\beta_n\beta_m\right)\times \mathrm{N} =$$

$$\sum_{m=-\infty}^{\infty}\sum_{n=-\infty}^{\infty}\left(\begin{array}{c}\omega\varepsilon_0 A_{nm}^{(e)}\dfrac{\left(\beta_{(1)}^{\,2}-\beta_m^{\,2}\right)}{\left(\beta_{(2)}^{\,2}-\beta_m^{\,2}\right)}\alpha_{nm}^{(2)} \\ +\dfrac{(\beta_n\beta_m)^2}{\omega\mu_0\alpha_{nm}^{(2)}}\dfrac{\left(\beta_{(2)}^{\,2}-\beta_{(1)}^{\,2}\right)}{\left(\beta_{(2)}^{\,2}-\beta_m^{\,2}\right)}A_{nm}^{(e)} \\ +j\dfrac{\alpha_{nm}^{(1)}}{\alpha_{nm}^{(2)}}A_{nm}^{(h)}\beta_n\beta_m\end{array}\right)\frac{\sinh\left(\alpha_{nm}^{(1)}d\right)}{\sinh\left(\alpha_{nm}^{(2)}(h-d)\right)}\times \mathrm{M} \qquad \text{(A1-26)}$$

$$\sum_{m=-\infty}^{\infty}\sum_{n=-\infty}^{\infty}\left(\begin{array}{c}-\omega\varepsilon_1 A_{nm}^{(e)}\sinh\left(\alpha_{nm}^{(1)}d\right)\alpha_{nm}^{(1)} - \\ jA_{nm}^{(h)}\sinh\left(\alpha_{nm}^{(1)}d\right)\beta_n\beta_m\end{array}\right)\coth(\alpha_{nm}^{(1)}y)e^{-j\beta_n x}e^{-j\beta_m z} =$$

$$\sum_{m=-\infty}^{\infty}\sum_{n=-\infty}^{\infty}\left(\begin{array}{c}\omega\varepsilon_0 A_{nm}^{(e)}\sinh\left(\alpha_{nm}^{(1)}d\right)\dfrac{\left(\beta_{(1)}^{\,2}-\beta_m^{\,2}\right)}{\left(\beta_{(2)}^{\,2}-\beta_m^{\,2}\right)}\alpha_{nm}^{(2)} \\ \dfrac{(\beta_n\beta_m)^2}{\omega\mu_0\alpha_{nm}^{(2)}}\dfrac{\left(\beta_{(2)}^{\,2}-\beta_{(1)}^{\,2}\right)}{\left(\beta_{(2)}^{\,2}-\beta_m^{\,2}\right)}A_{nm}^{(e)}\sinh\left(\alpha_{nm}^{(1)}d\right) \\ +j\dfrac{\alpha_{nm}^{(1)}}{\alpha_{nm}^{(2)}}A_{nm}^{(h)}\sinh\left(\alpha_{nm}^{(1)}d\right)\beta_n\beta_m\end{array}\right)\coth(\alpha_{nm}^{(2)}(h-y))e^{-j\beta_n x}e^{-j\beta_m z} \qquad \text{(A1-27)}$$

$$\overline{A_{nm}^{(e)}} = A_{nm}^{(e)}\sinh\left(\alpha_{nm}^{(1)}d\right) \qquad \text{(A1-28)}$$

$$\sum_{m=-\infty}^{\infty}\sum_{n=-\infty}^{\infty}\left(-\omega\varepsilon_1\overline{A_{nm}^{(e)}}\alpha_{nm}^{(1)} - jA_{nm}^{(h)}\sinh\left(\alpha_{nm}^{(1)}d\right)\beta_n\beta_m\right)\coth(\alpha_{nm}^{(1)}y)e^{-j\beta_n x}e^{-j\beta_m z} =$$

$$\sum_{m=-\infty}^{\infty}\sum_{n=-\infty}^{\infty}\left(\begin{array}{c}\omega\varepsilon_0\overline{A_{nm}^{(e)}}\dfrac{\left(\beta_{(1)}^{\,2}-\beta_m^{\,2}\right)}{\left(\beta_{(2)}^{\,2}-\beta_m^{\,2}\right)}\alpha_{nm}^{(2)} + \\ \dfrac{(\beta_n\beta_m)^2}{\omega\mu_0\alpha_{nm}^{(2)}}\dfrac{\left(\beta_{(2)}^{\,2}-\beta_{(1)}^{\,2}\right)}{\left(\beta_{(2)}^{\,2}-\beta_m^{\,2}\right)}\overline{A_{nm}^{(e)}} + \\ +j\dfrac{\alpha_{nm}^{(1)}}{\alpha_{nm}^{(2)}}A_{nm}^{(h)}\sinh\left(\alpha_{nm}^{(1)}d\right)\beta_n\beta_m\end{array}\right)\coth(\alpha_{nm}^{(2)}(h-y))e^{-j\beta_n x}e^{-j\beta_m z} \qquad \text{(A1-29)}$$

$$\sum_{m=-\infty}^{\infty}\sum_{n=-\infty}^{\infty}\left(\begin{array}{l}-\omega\varepsilon_1\overline{A_{nm}^{(e)}}\alpha_{nm}^{(1)}\coth(\alpha_{nm}^{(1)}y)e^{-j\beta_n x}e^{-j\beta_m z}- \\ \quad jA_{nm}^{(h)}\sinh(\alpha_{nm}^{(1)}d)\beta_n\beta_m\coth(\alpha_{nm}^{(1)}y)e^{-j\beta_n x}e^{-j\beta_m z}\end{array}\right)=$$

$$\sum_{m=-\infty}^{\infty}\sum_{n=-\infty}^{\infty}\left(\begin{array}{l}\omega\varepsilon_0\overline{A_{nm}^{(e)}}\dfrac{\left(\beta_{(1)}^{\ 2}-\beta_m^{\ 2}\right)}{\left(\beta_{(2)}^{\ 2}-\beta_m^{\ 2}\right)}\alpha_{nm}^{(2)}\coth(\alpha_{nm}^{(2)}(h-y))e^{-j\beta_n x}e^{-j\beta_m z} \\ \quad+\dfrac{(\beta_n\beta_m)^2}{\omega\mu_0\alpha_{nm}^{(2)}}\dfrac{\left(\beta_{(2)}^{\ 2}-\beta_{(1)}^{\ 2}\right)}{\left(\beta_{(2)}^{\ 2}-\beta_m^{\ 2}\right)}\overline{A_{nm}^{(e)}}\coth(\alpha_{nm}^{(2)}(h-y))e^{-j\beta_n x}e^{-j\beta_m z} \\ \quad\quad+j\dfrac{\alpha_{nm}^{(1)}}{\alpha_{nm}^{(2)}}A_{nm}^{(h)}\sinh(\alpha_{nm}^{(1)}d)\beta_n\beta_m\coth(\alpha_{nm}^{(2)}(h-y))e^{-j\beta_n x}e^{-j\beta_m z}\end{array}\right) \quad \text{(A1-30)}$$

$$\sum_{m=-\infty}^{\infty}\sum_{n=-\infty}^{\infty}\left(\begin{array}{l}-j\dfrac{\alpha_{nm}^{(1)}}{\alpha_{nm}^{(2)}}A_{nm}^{(h)}\sinh(\alpha_{nm}^{(1)}d)\beta_n\beta_m\coth(\alpha_{nm}^{(2)}(h-y))e^{-j\beta_n x}e^{-j\beta_m z} \\ \quad -jA_{nm}^{(h)}\sinh(\alpha_{nm}^{(1)}d)\beta_n\beta_m\coth(\alpha_{nm}^{(1)}y)e^{-j\beta_n x}e^{-j\beta_m z}\end{array}\right)=$$

$$\sum_{m=-\infty}^{\infty}\sum_{n=-\infty}^{\infty}\left(\begin{array}{l}\omega\varepsilon_0\overline{A_{nm}^{(e)}}\dfrac{\left(\beta_{(1)}^{\ 2}-\beta_m^{\ 2}\right)}{\left(\beta_{(2)}^{\ 2}-\beta_m^{\ 2}\right)}\alpha_{nm}^{(2)}\coth(\alpha_{nm}^{(2)}(h-y))e^{-j\beta_n x}e^{-j\beta_m z} \\ \quad+\dfrac{(\beta_n\beta_m)^2}{\omega\mu_0\alpha_{nm}^{(2)}}\dfrac{\left(\beta_{(2)}^{\ 2}-\beta_{(1)}^{\ 2}\right)}{\left(\beta_{(2)}^{\ 2}-\beta_m^{\ 2}\right)}\overline{A_{nm}^{(e)}}\coth(\alpha_{nm}^{(2)}(h-y))e^{-j\beta_n x}e^{-j\beta_m z} \\ \quad\quad+\omega\varepsilon_1\overline{A_{nm}^{(e)}}\alpha_{nm}^{(1)}\coth(\alpha_{nm}^{(1)}y)e^{-j\beta_n x}e^{-j\beta_m z}\end{array}\right) \quad \text{(A1-31)}$$

$$\sum_{m=-\infty}^{\infty}\sum_{n=-\infty}^{\infty}\left(\begin{array}{l}-\dfrac{\alpha_{nm}^{(1)}}{\alpha_{nm}^{(2)}}\beta_n\beta_m\coth(\alpha_{nm}^{(2)}(h-y)) \\ \quad -\beta_n\beta_m\coth(\alpha_{nm}^{(1)}y)\end{array}\right)jA_{nm}^{(h)}\sinh(\alpha_{nm}^{(1)}d)e^{-j\beta_n x}e^{-j\beta_m z}=$$

$$\sum_{m=-\infty}^{\infty}\sum_{n=-\infty}^{\infty}\left(\begin{array}{l}\omega\varepsilon_0\dfrac{\left(\beta_{(1)}^{\ 2}-\beta_m^{\ 2}\right)}{\left(\beta_{(2)}^{\ 2}-\beta_m^{\ 2}\right)}\alpha_{nm}^{(2)}\coth(\alpha_{nm}^{(2)}(h-y)) \\ \quad+\dfrac{(\beta_n\beta_m)^2}{\omega\mu_0\alpha_{nm}^{(2)}}\dfrac{\left(\beta_{(2)}^{\ 2}-\beta_{(1)}^{\ 2}\right)}{\left(\beta_{(2)}^{\ 2}-\beta_m^{\ 2}\right)}\coth(\alpha_{nm}^{(2)}(h-y))\overline{A_{nm}^{(e)}}e^{-j\beta_n x}e^{-j\beta_m z} \\ \quad\quad+\omega\varepsilon_1\alpha_{nm}^{(1)}\coth(\alpha_{nm}^{(1)}y)\end{array}\right) \quad \text{(A1-32)}$$

$$\sum_{m=-\infty}^{\infty}\sum_{n=-\infty}^{\infty} j\left(\begin{array}{l}\dfrac{\beta_n\beta_m}{\alpha_{nm}^{(2)}}\coth(\alpha_{nm}^{(2)}(h-y))\\ +\dfrac{\beta_n\beta_m}{\alpha_{nm}^{(1)}}\coth(\alpha_{nm}^{(1)}y)\end{array}\right)\omega\mu_0\frac{\alpha_{nm}^{(1)}}{\beta_n\beta_m}A_{nm}^{(h)}\sinh\left(\alpha_{nm}^{(1)}d\right)e^{-j\beta_n x}e^{-j\beta_m z}=$$

$$\sum_{m=-\infty}^{\infty}\sum_{n=-\infty}^{\infty}\left(\begin{array}{l}\dfrac{\omega^2\mu_0\varepsilon_0}{\beta_n\beta_m}\dfrac{\left(\beta_{(1)}^{\ 2}-\beta_m^{\ 2}\right)}{\left(\beta_{(2)}^{\ 2}-\beta_m^{\ 2}\right)}\alpha_{nm}^{(2)}\coth(\alpha_{nm}^{(2)}(h-y))\\ \quad+\dfrac{\beta_n\beta_m}{\alpha_{nm}^{(2)}}\dfrac{\left(\beta_{(2)}^{\ 2}-\beta_{(1)}^{\ 2}\right)}{\left(\beta_{(2)}^{\ 2}-\beta_m^{\ 2}\right)}\coth(\alpha_{nm}^{(2)}(h-y))\\ \quad\quad+\dfrac{\omega^2\mu_0\varepsilon_1}{\beta_n\beta_m}\alpha_{nm}^{(1)}\coth(\alpha_{nm}^{(1)}y)\end{array}\right)\overline{A_{nm}^{(e)}}e^{-j\beta_n x}e^{-j\beta_m z} \tag{A1-33}$$

$$\overline{A_{nm}^{(h)}}=j\omega\mu_0\frac{\alpha_{nm}^{(1)}}{\beta_n\beta_m}A_{nm}^{(h)}\sinh\left(\alpha_{nm}^{(1)}d\right) \tag{A1-34}$$

$$\sum_{m=-\infty}^{\infty}\sum_{n=-\infty}^{\infty}\left(\frac{\beta_n}{\alpha_{nm}^{(2)}}\coth(\alpha_{nm}^{(2)}(h-y))+\frac{\beta_n}{\alpha_{nm}^{(1)}}\coth(\alpha_{nm}^{(1)}y)\right)\overline{A_{nm}^{(h)}}e^{-j\beta_n x}e^{-j\beta_m z}=$$

$$\sum_{m=-\infty}^{\infty}\sum_{n=-\infty}^{\infty}\left(\begin{array}{l}\dfrac{\omega^2\mu_0\varepsilon_0}{\beta_n\beta_m^{\ 2}}\dfrac{\left(\beta_{(1)}^{\ 2}-\beta_m^{\ 2}\right)}{\left(\beta_{(2)}^{\ 2}-\beta_m^{\ 2}\right)}\alpha_{nm}^{(2)}\coth(\alpha_{nm}^{(2)}(h-y))\\ \quad+\dfrac{\beta_n}{\alpha_{nm}^{(2)}}\dfrac{\left(\beta_{(2)}^{\ 2}-\beta_{(1)}^{\ 2}\right)}{\left(\beta_{(2)}^{\ 2}-\beta_m^{\ 2}\right)}\coth(\alpha_{nm}^{(2)}(h-y))\\ \quad\quad+\dfrac{\omega^2\mu_0\varepsilon_1}{\beta_n\beta_m^{\ 2}}\alpha_{nm}^{(1)}\coth(\alpha_{nm}^{(1)}y)\end{array}\right)\overline{A_{nm}^{(e)}}e^{-j\beta_n x}e^{-j\beta_m z} \tag{A1-35}$$

$$T_{nm}(\beta_z)=\frac{\beta_n}{\alpha_{nm}^{(2)}}\coth(\alpha_{nm}^{(2)}(h-y))+\frac{\beta_n}{\alpha_{nm}^{(1)}}\coth(\alpha_{nm}^{(1)}y) \tag{A1-36}$$

$$\begin{aligned}P_{nm}(\beta_z)=&\frac{\omega^2\mu_0\varepsilon_0}{\beta_n\beta_m^{\ 2}}\frac{\left(\beta_{(1)}^{\ 2}-\beta_m^{\ 2}\right)}{\left(\beta_{(2)}^{\ 2}-\beta_m^{\ 2}\right)}\alpha_{nm}^{(2)}\coth(\alpha_{nm}^{(2)}(h-y))\\ &+\frac{\beta_n}{\alpha_{nm}^{(2)}}\frac{\left(\beta_{(2)}^{\ 2}-\beta_{(1)}^{\ 2}\right)}{\left(\beta_{(2)}^{\ 2}-\beta_m^{\ 2}\right)}\coth(\alpha_{nm}^{(2)}(h-y))+\frac{\omega^2\mu_0\varepsilon_1}{\beta_n\beta_m^{\ 2}}\alpha_{nm}^{(1)}\coth(\alpha_{nm}^{(1)}y)\end{aligned} \tag{A1-37}$$

$$\sum_{m=-\infty}^{\infty}\sum_{n=-\infty}^{\infty}P_{nm}(\beta_z)\overline{A_{nm}^{(e)}}e^{-j\beta_n x}e^{-j\beta_m z}+\sum_{m=-\infty}^{\infty}\sum_{n=-\infty}^{\infty}jT_{nm}(\beta_z)\overline{A_{nm}^{(h)}}e^{-j\beta_n x}e^{-j\beta_m z}=0 \tag{A1-38}$$

A.5. Condition 4 (a)

$$E_{x1}=0 \tag{A1-39}$$

$$\sum_{m=-\infty}^{\infty}\sum_{n=-\infty}^{\infty}\left(\omega\mu_0 A_{nm}^{(h)}\alpha_{nm} - jA_{nm}^{(e)}\beta_n\beta_m\right)\sinh(\alpha_{nm}^{(1)}y)e^{-j\beta_n x}e^{-j\beta_m z} = 0 \tag{A1-40}$$

$$\omega\mu_0\sum_{m=-\infty}^{\infty}\sum_{n=-\infty}^{\infty}A_{nm}^{(h)}\alpha_{nm}^{(1)}\sinh(\alpha_{nm}^{(1)}d)e^{-j\beta_n x}e^{-j\beta_m z} - j\sum_{m=-\infty}^{\infty}\sum_{n=-\infty}^{\infty}A_{nm}^{(e)}\beta_n\beta_m\sinh(\alpha_{nm}^{(1)}d)e^{-j\beta_n x}e^{-j\beta_m z} = 0 \tag{A1-41}$$

$$j\sum_{m=-\infty}^{\infty}\sum_{n=-\infty}^{\infty}\beta_n\beta_m\overline{A_{nm}^{(h)}}e^{-j\beta_n x}e^{-j\beta_m z} + \sum_{m=-\infty}^{\infty}\sum_{n=-\infty}^{\infty}\overline{A_{nm}^{(e)}}\beta_n\beta_m e^{-j\beta_n x}e^{-j\beta_m z} = 0 \tag{A1-42}$$

$$\sum_{m=-\infty}^{\infty}\sum_{n=-\infty}^{\infty}\overline{A_{nm}^{(e)}}\beta_n\beta_m e^{-j\beta_n x}e^{-j\beta_m z} + j\sum_{m=-\infty}^{\infty}\sum_{n=-\infty}^{\infty}\beta_n\beta_m\overline{A_{nm}^{(h)}}e^{-j\beta_n x}e^{-j\beta_m z} = 0 \tag{A1-43}$$

A.6. Condition 4 (b)

$$H_{z1} = H_{z2} \tag{A1-44}$$

$$\mathrm{M} = \cosh(\alpha_{nm}^{(2)}(h-y))e^{-j\beta_n x}e^{-j\beta_m z}$$

$$\mathrm{N} = \cosh(\alpha_{nm}^{(1)}y)e^{-j\beta_n x}e^{-j\beta_m z} \tag{A1-45a,b}$$

$$j\sum_{n=-\infty}^{\infty}\sum_{n=-\infty}^{\infty}\left(\beta_{(1)}^{\ 2}-\beta_m^{\ 2}\right)A_{nm}^{(h)}\cosh\left(\alpha_{nm}^{(1)}d\right)e^{-j\beta_n x}e^{-j\beta_m z} = j\sum_{n=-\infty}^{\infty}\sum_{n=-\infty}^{\infty}\left(\beta_{(2)}^{\ 2}-\beta_m^{\ 2}\right)B_{nm}^{(h)}\cosh\left(\alpha_{nm}^{(2)}(h-d)\right)e^{-j\beta_n x}e^{-j\beta_m z} \tag{A1-46}$$

$$\sum_{n=-\infty}^{\infty}\sum_{n=-\infty}^{\infty}\left(\beta_{(1)}^{\ 2}-\beta_m^{\ 2}\right)A_{nm}^{(h)}\times\mathrm{N} = \sum_{n=-\infty}^{\infty}\sum_{n=-\infty}^{\infty}\left(\beta_{(2)}^{\ 2}-\beta_m^{\ 2}\right)B_{nm}^{(h)}\times\mathrm{M} \tag{A1-47}$$

$$\sum_{n=-\infty}^{\infty}\sum_{n=-\infty}^{\infty}\left(\beta_{(1)}^{\ 2}-\beta_m^{\ 2}\right)A_{nm}^{(h)}\times\mathrm{N} = \sum_{n=-\infty}^{\infty}\sum_{n=-\infty}^{\infty}\left(\beta_{(2)}^{\ 2}-\beta_m^{\ 2}\right)\left(\begin{array}{c}\dfrac{j\beta_n\beta_m}{\omega\mu_0\alpha_{nm}^{(2)}}\dfrac{\left(\beta_{(2)}^{\ 2}-\beta_{(1)}^{\ 2}\right)}{\left(\beta_{(2)}^{\ 2}-\beta_m^{\ 2}\right)}A_{nm}^{(e)} \\ -\dfrac{\alpha_{nm}^{(1)}}{\alpha_{nm}^{(2)}}A_{nm}^{(h)}\end{array}\right)\frac{\sinh\left(\alpha_{nm}^{(1)}d\right)}{\sinh\left(\alpha_{nm}^{(2)}(h-d)\right)}\times\mathrm{M} \tag{A1-48}$$

$$\sum_{n=-\infty}^{\infty}\sum_{n=-\infty}^{\infty}\left(\beta_{(1)}{}^{2}-\beta_{m}{}^{2}\right)A_{nm}{}^{(h)}\coth\left(\alpha_{nm}{}^{(1)}d\right)e^{-j\beta_n x}e^{-j\beta_m z}=$$

$$\sum_{n=-\infty}^{\infty}\sum_{n=-\infty}^{\infty}\left(\beta_{(2)}{}^{2}-\beta_{m}{}^{2}\right)\left(\begin{array}{c}\dfrac{j\beta_n\beta_m}{\omega\mu_0\alpha_{nm}{}^{(2)}}\dfrac{\left(\beta_{(2)}{}^{2}-\beta_{(1)}{}^{2}\right)}{\left(\beta_{(2)}{}^{2}-\beta_{m}{}^{2}\right)}A_{nm}{}^{(e)}\\ -\dfrac{\alpha_{nm}{}^{(1)}}{\alpha_{nm}{}^{(2)}}A_{nm}{}^{(h)}\end{array}\right)\coth\left(\alpha_{nm}{}^{(2)}(h-d)\right) \qquad \text{(A1-49)}$$

$$\times e^{-j\beta_n x}e^{-j\beta_m z}$$

$$\mathrm{O}=\coth\left(\alpha_{nm}{}^{(2)}(h-d)\right)e^{-j\beta_n x}e^{-j\beta_m z}$$

$$\Pi=\coth\left(\alpha_{nm}{}^{(1)}d\right)e^{-j\beta_n x}e^{-j\beta_m z}$$

$$\sum_{n=-\infty}^{\infty}\sum_{n=-\infty}^{\infty}\left(\beta_{(1)}{}^{2}-\beta_{m}{}^{2}\right)A_{nm}{}^{(h)}\sinh\left(\alpha_{nm}{}^{(1)}d\right)\times\Pi=$$

$$\sum_{n=-\infty}^{\infty}\sum_{n=-\infty}^{\infty}\left(\beta_{(2)}{}^{2}-\beta_{m}{}^{2}\right)\left(\begin{array}{c}\dfrac{j\beta_n\beta_m}{\omega\mu_0\alpha_{nm}{}^{(2)}}\dfrac{\left(\beta_{(2)}{}^{2}-\beta_{(1)}{}^{2}\right)}{\left(\beta_{(2)}{}^{2}-\beta_{m}{}^{2}\right)}A_{nm}{}^{(e)}\sinh\left(\alpha_{nm}{}^{(1)}d\right)\\ -\dfrac{\alpha_{nm}{}^{(1)}}{\alpha_{nm}{}^{(2)}}A_{nm}{}^{(h)}\sinh\left(\alpha_{nm}{}^{(1)}d\right)\end{array}\right)\times\mathrm{O} \qquad \text{(A1-50)}$$

$$\sum_{n=-\infty}^{\infty}\sum_{n=-\infty}^{\infty}\left(\beta_{(1)}{}^{2}-\beta_{m}{}^{2}\right)A_{nm}{}^{(h)}\sinh\left(\alpha_{nm}{}^{(1)}d\right)\times\Pi=$$

$$\sum_{n=-\infty}^{\infty}\sum_{n=-\infty}^{\infty}\left(\beta_{(2)}{}^{2}-\beta_{m}{}^{2}\right)\left(\begin{array}{c}\dfrac{j\beta_n\beta_m}{\omega\mu_0\alpha_{nm}{}^{(2)}}\dfrac{\left(\beta_{(2)}{}^{2}-\beta_{(1)}{}^{2}\right)}{\left(\beta_{(2)}{}^{2}-\beta_{m}{}^{2}\right)}A_{nm}{}^{(e)}\sinh\left(\alpha_{nm}{}^{(1)}d\right)\\ -\dfrac{\alpha_{nm}{}^{(1)}}{\alpha_{nm}{}^{(2)}}A_{nm}{}^{(h)}\sinh\left(\alpha_{nm}{}^{(1)}d\right)\end{array}\right)\times\mathrm{O} \qquad \text{(A1-51)}$$

$$\overline{A_{nm}{}^{(e)}}=A_{nm}{}^{(e)}\sinh\left(\alpha_{nm}{}^{(1)}d\right) \qquad \text{(A1-52)}$$

$$\sum_{n=-\infty}^{\infty}\sum_{n=-\infty}^{\infty}\left(\beta_{(1)}{}^{2}-\beta_{m}{}^{2}\right)A_{nm}{}^{(h)}\sinh\left(\alpha_{nm}{}^{(1)}d\right)\coth\left(\alpha_{nm}{}^{(1)}d\right)e^{-j\beta_n x}e^{-j\beta_m z}=$$

$$\sum_{n=-\infty}^{\infty}\sum_{n=-\infty}^{\infty}\left(\beta_{(2)}{}^{2}-\beta_{m}{}^{2}\right)\left(\begin{array}{c}\dfrac{j\beta_n\beta_m}{\omega\mu_0\alpha_{nm}{}^{(2)}}\dfrac{\left(\beta_{(2)}{}^{2}-\beta_{(1)}{}^{2}\right)}{\left(\beta_{(2)}{}^{2}-\beta_{m}{}^{2}\right)}\overline{A_{nm}{}^{(e)}}\\ -\dfrac{\alpha_{nm}{}^{(1)}}{\alpha_{nm}{}^{(2)}}A_{nm}{}^{(h)}\sinh\left(\alpha_{nm}{}^{(1)}d\right)\end{array}\right)\coth\left(\alpha_{nm}{}^{(2)}(h-d)\right) \qquad \text{(A1-53)}$$

$$\times e^{-j\beta_n x}e^{-j\beta_m z}$$

$$\sum_{n=-\infty}^{\infty}\sum_{n=-\infty}^{\infty}\left(\begin{array}{l}\left(\beta_{(1)}{}^2-\beta_m{}^2\right)A_{nm}{}^{(h)}\sinh\left(\alpha_{nm}{}^{(1)}d\right)\coth\left(\alpha_{nm}{}^{(1)}d\right)e^{-j\beta_n x}e^{-j\beta_m z}\\ +\left(\beta_{(2)}{}^2-\beta_m{}^2\right)\left(\frac{\alpha_{nm}{}^{(1)}}{\alpha_{nm}{}^{(2)}}A_{nm}{}^{(h)}\sinh\left(\alpha_{nm}{}^{(1)}d\right)\right)\coth\left(\alpha_{nm}{}^{(2)}(h-d)\right)\\ \qquad\qquad\times e^{-j\beta_n x}e^{-j\beta_m z}\end{array}\right) \tag{A1-54}$$

$$=\sum_{n=-\infty}^{\infty}\sum_{n=-\infty}^{\infty}\left(\frac{j\beta_n\beta_m}{\omega\mu_0\alpha_{nm}{}^{(2)}}\left(\beta_{(2)}{}^2-\beta_{(1)}{}^2\right)\right)\overline{A_{nm}{}^{(e)}}\coth\left(\alpha_{nm}{}^{(2)}(h-d)\right)e^{-j\beta_n x}e^{-j\beta_m z}$$

$$\sum_{n=-\infty}^{\infty}\sum_{n=-\infty}^{\infty}\left(\begin{array}{l}\left(\beta_{(1)}{}^2-\beta_m{}^2\right)\coth\left(\alpha_{nm}{}^{(1)}d\right)+\\ \left(\beta_{(2)}{}^2-\beta_m{}^2\right)\frac{\alpha_{nm}{}^{(1)}}{\alpha_{nm}{}^{(2)}}\coth\left(\alpha_{nm}{}^{(2)}(h-d)\right)\end{array}\right)A_{nm}{}^{(h)}\sinh\left(\alpha_{nm}{}^{(1)}d\right)e^{-j\beta_n x}e^{-j\beta_m z}=$$

$$\sum_{n=-\infty}^{\infty}\sum_{n=-\infty}^{\infty}\left(\frac{j\beta_n\beta_m}{\omega\mu_0\alpha_{nm}{}^{(2)}}\left(\beta_{(2)}{}^2-\beta_{(1)}{}^2\right)\right)\overline{A_{nm}{}^{(e)}}\coth\left(\alpha_{nm}{}^{(2)}(h-d)\right)e^{-j\beta_n x}e^{-j\beta_m z} \tag{A1-55}$$

$$\overline{A_{nm}{}^{(h)}}=\omega\mu_0\frac{\alpha_{nm}{}^{(1)}}{\beta_n\beta_m}A_{nm}{}^{(h)}\sinh\left(\alpha_{nm}{}^{(1)}d\right) \tag{A1-56}$$

$$-j\sum_{n=-\infty}^{\infty}\sum_{n=-\infty}^{\infty}\left(\begin{array}{l}\frac{\beta_n\beta_m}{\alpha_{nm}{}^{(1)}}\left(\beta_{(1)}{}^2-\beta_m{}^2\right)\coth\left(\alpha_{nm}{}^{(1)}d\right)\\ \qquad+\left(\beta_{(2)}{}^2-\beta_m{}^2\right)\frac{\beta_n\beta_m}{\alpha_{nm}{}^{(2)}}\coth\left(\alpha_{nm}{}^{(2)}(h-d)\right)\end{array}\right)\overline{A_{nm}{}^{(h)}}e^{-j\beta_n x}e^{-j\beta_m z}=$$

$$\sum_{n=-\infty}^{\infty}\sum_{n=-\infty}^{\infty}\left(\frac{\beta_n\beta_m}{\alpha_{nm}{}^{(2)}}\left(\beta_{(2)}{}^2-\beta_{(1)}{}^2\right)\right)\overline{A_{nm}{}^{(e)}}\coth\left(\alpha_{nm}{}^{(2)}(h-d)\right)e^{-j\beta_n x}e^{-j\beta_m z} \tag{A1-57}$$

$$-j\sum_{n=-\infty}^{\infty}\sum_{n=-\infty}^{\infty}\left(\begin{array}{l}\frac{\beta_n\beta_m}{\alpha_{nm}{}^{(1)}}\left(\beta_{(1)}{}^2-\beta_m{}^2\right)\coth\left(\alpha_{nm}{}^{(1)}d\right)+\\ \qquad\left(\beta_{(2)}{}^2-\beta_m{}^2\right)\frac{\beta_n\beta_m}{\alpha_{nm}{}^{(2)}}\coth\left(\alpha_{nm}{}^{(2)}(h-d)\right)\end{array}\right)\overline{A_{nm}{}^{(h)}}e^{-j\beta_n x}e^{-j\beta_m z}=$$

$$\sum_{n=-\infty}^{\infty}\sum_{n=-\infty}^{\infty}\left(\frac{\beta_n\beta_m}{\alpha_{nm}{}^{(2)}}\left(\beta_{(2)}{}^2-\beta_{(1)}{}^2\right)\right)\overline{A_{nm}{}^{(e)}}\coth\left(\alpha_{nm}{}^{(2)}(h-d)\right)e^{-j\beta_n x}e^{-j\beta_m z} \tag{A1-58}$$

$$-j\sum_{n=-\infty}^{\infty}\sum_{n=-\infty}^{\infty}\left(\begin{array}{l}\frac{\beta_n\beta_m}{\alpha_{nm}^{(1)}}\left(\beta_{(1)}{}^2-\beta_m{}^2\right)\coth\left(\alpha_{nm}{}^{(1)}d\right)+\\ \qquad\left(\beta_{(2)}{}^2-\beta_m{}^2\right)\frac{\beta_n\beta_m}{\alpha_{nm}^{(2)}}\coth\left(\alpha_{nm}{}^{(2)}(h-d)\right)\end{array}\right)\overline{A_{nm}{}^{(h)}}e^{-j\beta_n x}e^{-j\beta_m z}=$$

$$\sum_{n=-\infty}^{\infty}\sum_{n=-\infty}^{\infty}\left(\frac{\beta_n\beta_m}{\alpha_{nm}^{(2)}}\left(\beta_{(2)}{}^2-\beta_{(1)}{}^2\right)\right)\overline{A_{nm}{}^{(e)}}\coth\left(\alpha_{nm}{}^{(2)}(h-d)\right)e^{-j\beta_n x}e^{-j\beta_m z} \tag{A1-59}$$

$$W_n(\beta_z)=\left(\begin{array}{l}\frac{\beta_n\beta_m}{\alpha_{nm}^{(1)}}\left(\beta_{(1)}{}^2-\beta_m{}^2\right)\coth\left(\alpha_{nm}{}^{(1)}d\right)+\\ \qquad\left(\beta_{(2)}{}^2-\beta_m{}^2\right)\frac{\beta_n\beta_m}{\alpha_{nm}^{(2)}}\coth\left(\alpha_{nm}{}^{(2)}(h-d)\right)\end{array}\right) \tag{A1-60}$$

$$Q_n(\beta_z)=\left(\frac{\beta_n\beta_m}{\alpha_{nm}^{(2)}}\left(\beta_{(2)}{}^2-\beta_{(1)}{}^2\right)\right)\coth\left(\alpha_{nm}{}^{(2)}(h-d)\right) \tag{A1-61}$$

$$\sum_{n=-\infty}^{\infty}\sum_{n=-\infty}^{\infty}Q_n(\beta_z)\overline{A_{nm}{}^{(e)}}e^{-j\beta_n x}e^{-j\beta_m z}+j\sum_{n=-\infty}^{\infty}\sum_{n=-\infty}^{\infty}W_n(\beta_z)\overline{A_{nm}{}^{(h)}}e^{-j\beta_n x}e^{-j\beta_m z}=0 \tag{A1-62}$$

Appendix B

MATLAB CODE

B.1. sitsodominant.m

```
clc
clear all;
close all;
%tt=cputime;

fmax=50e9;
fmin=20e9;
N=7;

% GEOMETERY OF THE PROBLEM
L = 20e-3;      %The half length of the shield along x-direction
h = 20.0e-3;     %The length of the shield along y-direction
d = 1.5478e-3;        %The thickness of the substrate along y-direction
t = 0.5*5.0e-3;       %The half width of the strip

%CONSTITUATIVE PARAMETERS
epsilon0=1e-9/36/pi;
miu0=pi*4.0e-7;
epsilonr=8.8;

%NORMALIZATION
Num=50;
f=linspace(fmax,fmin,Num);

  k0=2*pi*f*sqrt(epsilon0*miu0);
  kr=2*pi*f*sqrt(epsilonr*epsilon0*miu0);

  betax=0.0001;
  nL=L;
  nh=h;
  nd=d;
  nt=t;
  nbetax=betax;
```

```
  nbetaz0=4.0*k0;

  for i=1:Num

  for j=1:1
    fprintf('i = %d\t', i)
    fprintf('freq = %2.2dGHz\t', f(i)/1e9)

    %[nbetaz(i,j), fval] = fminsearch(@(betaz) temparef(betaz,nbetax(i), beta1, beta2,
nL(i), nh(i), nd(i), nt(i), epsilonr, Nx, Nz ) , [nbetaz0(j)]);

    [nbetaz(i,j), fval]=fminsearch('temparef2',nbetaz0(i),[],nbetax,k0(i), kr(i),
nL,nh,nd,nt,epsilonr,N);
    nbetaz0(j)=nbetaz(i,j);
    fprintf('fval = %d\t', fval)
    fprintf('nbetaz = %d\n', nbetaz0(j)/k0(i))

  end
  plot(f(1:i)/1e9 , nbetaz(1:i,1))
  xlabel('{\itf} (GHz)')
  ylabel('\beta_z')
  grid
  pause(2)
end
```

B.2. temparef2.m

```
function y = temparef2(betaz, betax, k0, kr, L, h, d, t,  N)

A1 = twodpointmatching(betaz, betax, k0, kr, L, h, d, t, N);
sm = svd(A1);
y = min(sm).^2;
```

B.3. twodpointmatching.m (normal case)

```
function A1=twodpointmatching(betaz, betax, k0, kr, L, h, d, t, N)

r = t / L;
j = sqrt(-1);

xNum1 = ceil((1 - r) * (2 * N + 1) / 2);
x1min = -L;
```

```
x1max = -t;
deltax1 = (x1max - x1min) / (xNum1 + 1);

xNum2 = 2 * N + 1 - 2 * xNum1;
x2min = -t;
x2max = t;
deltax2 = (x2max - x2min) / (xNum2 + 1);

xNum3 =ceil((1-r)*(2*N+1)/2);
x3min=t;
x3max=L;
deltax3=(x3max-x3min)/(xNum3+1);

zNum1 = ceil((1 - r) * (2 * N + 1) / 2);
z1min = -L;
z1max = -t;
deltaz1 = (z1max - z1min) / (zNum1 + 1);

zNum2 = 2 * N + 1 - 2 * zNum1;
z2min = -t;
z2max = t;
deltaz2 = (z2max - z2min) / (zNum2 + 1);

zNum3 =ceil((1-r)*(2*N+1)/2);
z3min=t;
z3max=L;
deltaz3=(z3max-z3min)/(zNum3+1);

for m =-N:N
  for n=-N:N
    betan=betax+n*pi/L;
    betam=betaz+ m*pi/L;

    if betan.^2+betam.^2>=kr.^2
      alphan1=sqrt(betan.^2+betam.^2-kr.^2);
    else
      alphan1=-j*sqrt(kr.^2-betan.^2-betam.^2);
    end

    if betan.^2+betam.^2>=1;
      alphan2=sqrt(betan.^2+betam.^2-k0.^2);
    else
      alphan2=-j*sqrt(k0.^2-betan.^2-betam.^2);
    end

    tempt1=coth(alphan1*d);
```

```
tempt2=coth(alphan2*(h-d));

if betan == 0 || betam == 0
  Pn = kr.^2 .* alphan1 .* tempt1 + (kr.^2 - betam.^2) / (k0.^2 - betam.^2) .*
alphan2 .* tempt2;
else
  Pn = kr.^2.* alphan1 ./ (betan .* betam) .* tempt1 ...
    + alphan2 .* tempt2 .* (k0.^2 - betam.^2) / (kr.^2 - betam.^2) ./ (betan .*
betam)...
    + betan .* betam ./ alphan2 .* (kr.^2 - k0.^2)/(kr.^2 - betam.^2).*tempt2;

end

Tn = betan .* betam ./ alphan1 .* tempt1 + betan .* betam ./ alphan2 .* tempt2;
Qn = betan .* betam ./ alphan2 .* (k0.^2 - kr.^2) ./ (k0.^2 - betam.^2).*tempt2;
Wn = (kr.^2 - betam.^2)./(k0.^2 - betam.^2) .* betan .* betam ./ alphan1 .* tempt1 +
betam .* betan ./ alphan2 .* tempt2;

q = n+N+1;
p = m+N+1;

    %REGION A

    for x = 1:xNum1
      x1 = x1min + x * deltax1;
      for z = 1:zNum1
        z1 = z1min + z * deltaz1;
        b = (p - 1) * (2*N+1) + q;
        a = (x - 1) * xNum1 + z;
        A1mn(a, b) = betan .* betam .* Pn * exp(-j * betan * x1) .* exp(-j * betam
* z1);
        A2mn(a, b) = betan .* betam .* Tn * exp(-j * betan * x1) .* exp(-j * betam
* z1);
        A3mn(a, b) = Qn * exp(-j * betan * x1) .* exp(-j * betam * z1);
        A4mn(a, b) = Wn * exp(-j * betan * x1) .* exp(-j * betam * z1);
      end
    end

    %REGION B

    for x = 1:xNum2
      x2 = x2min + x * deltax2;
      for z = 1:zNum1
        z1 = z1min + z * deltaz1;
        b = (p - 1) * (2*N+1) + q;
        a = (x - 1) * xNum2 + z;
```

```
            B1mn(a, b) = betan .* betam .* Pn * exp(-j * betan * x2) .* exp(-j * betam
* z1);
            B2mn(a, b) = betan .* betam .* Tn * exp(-j * betan * x2) .* exp(-j * betam
* z1);
            B3mn(a, b) = Qn * exp(-j * betan * x2) .* exp(-j * betam * z1);
            B4mn(a, b) = Wn * exp(-j * betan * x2) .* exp(-j * betam * z1);
          end
        end

        %REGION C

        for x = 1:xNum3
          x3 = x3min + x * deltax3;
          for z = 1:zNum1
            z1 = z1min + z * deltaz1;
            b = (p - 1) * (2*N+1) + q;
            a = (x - 1) * xNum3 + z;
            C1mn(a, b) = betan .* betam .* Pn * exp(-j * betan * x3) .* exp(-j * betam
* z1);
            C2mn(a, b) = betan .* betam .* Tn * exp(-j * betan * x3) .* exp(-j * betam
* z1);
            C3mn(a, b) = Qn * exp(-j * betan * x3) .* exp(-j * betam * z1);
            C4mn(a, b) = Wn * exp(-j * betan * x3) .* exp(-j * betam * z1);
          end
        end

         %REGION D

        for x = 1:xNum1
          x1 = x1min + x * deltax1;
          for z = 1:zNum2
            z2 = z2min + z * deltaz2;
            b = (p - 1) * (2*N+1) + q;
            a = (x - 1) * xNum1 + z;
            D1mn(a, b) = betan .* betam .* Pn * exp(-j * betan * x1) .* exp(-j * betam
* z2);
            D2mn(a, b) = betan .* betam .* Tn * exp(-j * betan * x1) .* exp(-j * betam
* z2);
            D3mn(a, b) = Qn * exp(-j * betan * x1) .* exp(-j * betam * z2);
            D4mn(a, b) = Wn * exp(-j * betan * x1) .* exp(-j * betam * z2);
          end
        end

        %REGION E

        for x = 1:xNum2
```

```
    x2 = x2min + x * deltax2;
    for z = 1:zNum2
      z2 = z2min + z * deltaz2;
      b = (p - 1) * (2*N+1) + q;
      a = (x - 1) * xNum2 + z;
      E1mn(a, b) = (kr.^2 - betam.^2) .* exp(-j * betan * x2) .* exp(-j * betam *
z2);
      E2mn(a, b) = 0;
      E3mn(a, b) = betan .* betam * exp(-j * betan * x2) .* exp(-j * betam * z2);
      E4mn(a, b) = betan .* betam * exp(-j * betan * x2) .* exp(-j * betam * z2);
    end
  end

  %REGION F

  for x = 1:xNum3
    x3 = x3min + x * deltax3;
    for z = 1:zNum2
      z2 = z2min + z * deltaz2;
      b = (p - 1) * (2*N+1) + q;
      a = (x - 1) * xNum3 + z;
      F1mn(a, b) = betan .* betam .* Pn * exp(-j * betan * x3) .* exp(-j * betam
* z2);
      F2mn(a, b) = betan .* betam .* Tn * exp(-j * betan * x3) .* exp(-j * betam
* z2);
      F3mn(a, b) = Qn * exp(-j * betan * x3) .* exp(-j * betam * z2);
      F4mn(a, b) = Wn * exp(-j * betan * x3) .* exp(-j * betam * z2);
    end
  end
  %REGION G

  for x = 1:xNum1
    x1 = x1min + x * deltax1;
    for z = 1:zNum3
      z3 = z3min + z * deltaz3;
      b = (p - 1) * (2*N+1) + q;
      a = (x - 1) * xNum1 + z;
      G1mn(a, b) = betan .* betam .* Pn * exp(-j * betan * x1) .* exp(-j * betam
* z3);
      G2mn(a, b) = betan .* betam .* Tn * exp(-j * betan * x1) .* exp(-j * betam
* z3);
      G3mn(a, b) = Qn * exp(-j * betan * x1) .* exp(-j * betam * z3);
      G4mn(a, b) = Wn * exp(-j * betan * x1) .* exp(-j * betam * z3);
    end
  end
```

```
            %REGION H

            for x = 1:xNum2
               x2 = x2min + x * deltax2;
               for z = 1:zNum3
                  z3 = z3min + z * deltaz3;
                  b = (p - 1) * (2*N+1) + q;
                  a = (x - 1) * xNum2 + z;
                  H1mn(a, b) = betan .* betam .* Pn * exp(-j * betan * x2) .* exp(-j * betam
* z3);
                  H2mn(a, b) = betan .* betam .* Tn * exp(-j * betan * x2) .* exp(-j * betam
* z3);
                  H3mn(a, b) = Qn * exp(-j * betan * x2) .* exp(-j * betam * z3);
                  H4mn(a, b) = Wn * exp(-j * betan * x2) .* exp(-j * betam * z3);
               end
            end

            %REGION I

            for x = 1:xNum3
               x3 = x3min + x * deltax3;
               for z = 1:zNum3
                  z3 = z3min + z * deltaz3;
                  b = (p - 1) * (2*N+1) + q;
                  a = (x - 1) * xNum1 + z;
                  I1mn(a, b) = betan .* betam .* Pn * exp(-j * betan * x3) .* exp(-j * betam
* z3);
                  I2mn(a, b) = betan .* betam .* Tn * exp(-j * betan * x3) .* exp(-j * betam
* z3);
                  I3mn(a, b) = Qn * exp(-j * betan * x3) .* exp(-j * betam * z3);
                  I4mn(a, b) = Wn * exp(-j * betan * x3) .* exp(-j * betam * z3);
               end
            end
      end
   end

   A = [A1mn, A2mn; A3mn, A4mn];
   B = [B1mn, B2mn; B3mn, B4mn];
   C = [C1mn, C2mn; C3mn, C4mn];

   D = [D1mn, D2mn; D3mn, D4mn];
   E = [E1mn, E2mn; E3mn, E4mn];
   F = [F1mn, F2mn; F3mn, F4mn];

   G = [G1mn, G2mn; G3mn, G4mn];
   H = [H1mn, H2mn; H3mn, H4mn];
```

```
I = [I1mn, I2mn; I3mn, I4mn];

A1 = [A;B;C;D;E;F;G;H;I];
```

B.4. twodpointmatching.m (limiting case)

```
function A1=twodpointmatching(betaz, betax, k0,kr,L, h, d, t, N)

zL = 1000*L;
zt = 1000*L;
zr = zt/zL;

r = t / L;
j = sqrt(-1);

xNum1 = ceil((1 - r) * (2 * N + 1) / 2);
x1min = -L;
x1max = -t;
deltax1 = (x1max - x1min) / (xNum1 + 1);

xNum2 = 2 * N + 1 - 2 * xNum1;
x2min = -t;
x2max = t;
deltax2 = (x2max - x2min) / (xNum2 + 1);

xNum3 =ceil((1-r)*(2*N+1)/2);
x3min=t;
x3max=L;
deltax3=(x3max-x3min)/(xNum3+1);

zNum1 = ceil((1 - zr) * (2 * N + 1) / 2);
z1min = -zL;
z1max = -zt;
deltaz1 = (z1max - z1min) / (zNum1 + 1);

zNum2 = 2 * N + 1 - 2 * zNum1;
z2min = -zt;
z2max = zt;
deltaz2 = (z2max - z2min) / (zNum2 + 1);

zNum3 =ceil((1-zr)*(2*N+1)/2);
z3min=zt;
z3max=zL;
deltaz3=(z3max-z3min)/(zNum3+1);
```

```
for m =-N:-N
  for n=-N:N
    betan=betax+n*pi/L;
    betam=betaz ;

    if betan.^2+betam.^2>=kr.^2
      alphan1=sqrt(betan.^2+betam.^2-kr.^2);
    else
      alphan1=-j*sqrt(kr.^2-betan.^2-betam.^2);
    end

    if betan.^2+betam.^2>=1;
      alphan2=sqrt(betan.^2+betam.^2-k0.^2);
    else
      alphan2=-j*sqrt(k0.^2-betan.^2-betam.^2);
    end

    tempt1=coth(alphan1*d);
    tempt2=coth(alphan2*(h-d));

    if betan == 0 || betam == 0
      Pn = kr.^2 .* alphan1 .* tempt1 + (kr.^2 - betam.^2) / (k0.^2 - betam.^2) .*
alphan2 .* tempt2;
    else
      Pn = kr.^2.* alphan1 ./ (betan .* betam) .* tempt1 ...
        + alphan2 .* tempt2 .* (k0.^2 - betam.^2) / (kr.^2 - betam.^2) ./ (betan .*
betam)...
        + betan .* betam ./ alphan2 .* (kr.^2 - k0.^2)/(kr.^2 - betam.^2).*tempt2;

    end

    Tn = betan .* betam ./ alphan1 .* tempt1 + betan .* betam ./ alphan2 .* tempt2;
    Qn = betan .* betam ./ alphan2 .* (k0.^2 - kr.^2) ./ (k0.^2 - betam.^2).*tempt2;
    Wn = (kr.^2 - betam.^2)./(k0.^2 - betam.^2) .* betan .* betam ./ alphan1 .* tempt1 +
betam .* betan ./ alphan2 .* tempt2;

    q = n+N+1;
    p = m+N+1;

      %REGION A

      for x = 1:xNum1
        x1 = x1min + x * deltax1;
        for z = 1:zNum1
          z1 = z1min + z * deltaz1;
```

```
            b = (p - 1) * (2*N+1) + q;
            a = (x - 1) * xNum1 + z;
            A1mn(a, b) = betan .* betam .* Pn * exp(-j * betan * x1) .* exp(-j * betam
* z1);
            A2mn(a, b) = betan .* betam .* Tn * exp(-j * betan * x1) .* exp(-j * betam
* z1);
            A3mn(a, b) = Qn * exp(-j * betan * x1) .* exp(-j * betam * z1);
            A4mn(a, b) = Wn * exp(-j * betan * x1) .* exp(-j * betam * z1);
          end
        end

        %REGION B

        for x = 1:xNum2
          x2 = x2min + x * deltax2;
          for z = 1:zNum1
            z1 = z1min + z * deltaz1;
            b = (p - 1) * (2*N+1) + q;
            a = (x - 1) * xNum2 + z;
            B1mn(a, b) = betan .* betam .* Pn * exp(-j * betan * x2) .* exp(-j * betam
* z1);
            B2mn(a, b) = betan .* betam .* Tn * exp(-j * betan * x2) .* exp(-j * betam
* z1);
            B3mn(a, b) = Qn * exp(-j * betan * x2) .* exp(-j * betam * z1);
            B4mn(a, b) = Wn * exp(-j * betan * x2) .* exp(-j * betam * z1);
          end
        end

        %REGION C

        for x = 1:xNum3
          x3 = x3min + x * deltax3;
          for z = 1:zNum1
            z1 = z1min + z * deltaz1;
            b = (p - 1) * (2*N+1) + q;
            a = (x - 1) * xNum3 + z;
            C1mn(a, b) = betan .* betam .* Pn * exp(-j * betan * x3) .* exp(-j * betam
* z1);
            C2mn(a, b) = betan .* betam .* Tn * exp(-j * betan * x3) .* exp(-j * betam
* z1);
            C3mn(a, b) = Qn * exp(-j * betan * x3) .* exp(-j * betam * z1);
            C4mn(a, b) = Wn * exp(-j * betan * x3) .* exp(-j * betam * z1);
          end
        end

         %REGION D
```

```
for x = 1:xNum1
   x1 = x1min + x * deltax1;
   for z = 1:zNum2
      z2 = z2min + z * deltaz2;
      b = (p - 1) * (2*N+1) + q;
      a = (x - 1) * xNum1 + z;
      D1mn(a, b) = betan .* betam .* Pn * exp(-j * betan * x1) .* exp(-j * betam
* z2);
      D2mn(a, b) = betan .* betam .* Tn * exp(-j * betan * x1) .* exp(-j * betam
* z2);
      D3mn(a, b) = Qn * exp(-j * betan * x1) .* exp(-j * betam * z2);
      D4mn(a, b) = Wn * exp(-j * betan * x1) .* exp(-j * betam * z2);
   end
end

%REGION E

for x = 1:xNum2
   x2 = x2min + x * deltax2;
   for z = 1:zNum2
      z2 = z2min + z * deltaz2;
      b = (p - 1) * (2*N+1) + q;
      a = (x - 1) * xNum2 + z;
      E1mn(a, b) = (kr.^2 - betam.^2) .* exp(-j * betan * x2) .* exp(-j * betam *
z2);
      E2mn(a, b) = 0;
      E3mn(a, b) = betan .* betam * exp(-j * betan * x2) .* exp(-j * betam * z2);
      E4mn(a, b) = betan .* betam * exp(-j * betan * x2) .* exp(-j * betam * z2);
   end
end

%REGION F

for x = 1:xNum3
   x3 = x3min + x * deltax3;
   for z = 1:zNum2
      z2 = z2min + z * deltaz2;
      b = (p - 1) * (2*N+1) + q;
      a = (x - 1) * xNum3 + z;
      F1mn(a, b) = betan .* betam .* Pn * exp(-j * betan * x3) .* exp(-j * betam
* z2);
      F2mn(a, b) = betan .* betam .* Tn * exp(-j * betan * x3) .* exp(-j * betam
* z2);
      F3mn(a, b) = Qn * exp(-j * betan * x3) .* exp(-j * betam * z2);
      F4mn(a, b) = Wn * exp(-j * betan * x3) .* exp(-j * betam * z2);
```

```
    end
  end
  %REGION G

  for x = 1:xNum1
    x1 = x1min + x * deltax1;
    for z = 1:zNum3
      z3 = z3min + z * deltaz3;
      b = (p - 1) * (2*N+1) + q;
      a = (x - 1) * xNum1 + z;
      G1mn(a, b) = betan .* betam .* Pn * exp(-j * betan * x1) .* exp(-j * betam
* z3);
      G2mn(a, b) = betan .* betam .* Tn * exp(-j * betan * x1) .* exp(-j * betam
* z3);
      G3mn(a, b) = Qn * exp(-j * betan * x1) .* exp(-j * betam * z3);
      G4mn(a, b) = Wn * exp(-j * betan * x1) .* exp(-j * betam * z3);
    end
  end

  %REGION H

  for x = 1:xNum2
    x2 = x2min + x * deltax2;
    for z = 1:zNum3
      z3 = z3min + z * deltaz3;
      b = (p - 1) * (2*N+1) + q;
      a = (x - 1) * xNum2 + z;
      H1mn(a, b) = betan .* betam .* Pn * exp(-j * betan * x2) .* exp(-j * betam
* z3);
      H2mn(a, b) = betan .* betam .* Tn * exp(-j * betan * x2) .* exp(-j * betam
* z3);
      H3mn(a, b) = Qn * exp(-j * betan * x2) .* exp(-j * betam * z3);
      H4mn(a, b) = Wn * exp(-j * betan * x2) .* exp(-j * betam * z3);
    end
  end

  %REGION I

  for x = 1:xNum3
    x3 = x3min + x * deltax3;
    for z = 1:zNum3
      z3 = z3min + z * deltaz3;
      b = (p - 1) * (2*N+1) + q;
      a = (x - 1) * xNum1 + z;
      I1mn(a, b) = betan .* betam .* Pn * exp(-j * betan * x3) .* exp(-j * betam
* z3);
```

```
                I2mn(a, b) = betan .* betam .* Tn * exp(-j * betan * x3) .* exp(-j * betam
* z3);
                I3mn(a, b) = Qn * exp(-j * betan * x3) .* exp(-j * betam * z3);
                I4mn(a, b) = Wn * exp(-j * betan * x3) .* exp(-j * betam * z3);
            end
        end
    end
end

if zNum1 ~= 0;

    A = [A1mn, A2mn; A3mn, A4mn];
    B = [B1mn, B2mn; B3mn, B4mn];
    C = [C1mn, C2mn; C3mn, C4mn];

    D = [D1mn, D2mn; D3mn, D4mn];
    E = [E1mn, E2mn; E3mn, E4mn];
    F = [F1mn, F2mn; F3mn, F4mn];

    G = [G1mn, G2mn; G3mn, G4mn];
    H = [H1mn, H2mn; H3mn, H4mn];
    I = [I1mn, I2mn; I3mn, I4mn];

    A1 = [A;B;C;D;E;F;G;H;I];
else
    D = [D1mn, D2mn; D3mn, D4mn];
    E = [E1mn, E2mn; E3mn, E4mn];
    F = [F1mn, F2mn; F3mn, F4mn];

    A1 = [D;E;F];
end
```

Appendix C

ADS SCHEMATICS